

illuminating Darkness: Enhancing Real-world Low-light Scenes with Smartphone Images

S M A Sharif¹, Abdur Rehman¹, Zain Ul Abidin², Rizwan Ali Naqvi^{2*},
Fayaz Ali Dharejo³, Radu Timofte^{3*}
¹Opt-AI Inc., ²Sejong University, ³University of Wurzburg,

Abstract

Digital cameras often struggle to produce plausible images in low-light conditions. Improving these single-shot images remains challenging due to a lack of diverse real-world pair data samples. To address this limitation, we propose a large-scale high-resolution (i.e., beyond 4k) pair Single-Shot Low-Light Enhancement (SLLIE) dataset. Our dataset comprises 6,425 unique focus-aligned image pairs captured with smartphone sensors in dynamic settings under challenging lighting conditions (0.1–200 lux), covering various indoor and outdoor scenes with varying noise and intensity. We extracted and refined around 180,000 non-overlapping patches from 6,025 collected scenes for training while reserving 400 pairs for benchmarking. In addition to that, we collected 2,117 low-light scenes from different sources for extensive real-world aesthetic evaluation. To our knowledge, this is the largest real-world dataset available for SLLIE research. We also propose learning luminance-chrominance (LC) attributes separately through a tuning fork-shaped transformer model to enhance real-world low-light images, addressing challenges like denoising and over-enhancement in complex scenes. We also propose an LC cross-attention block for feature fusion, an LC refinement block for enhanced reconstruction, and LC-guided supervision to ensure perceptually coherent enhancements. We demonstrated our method’s effectiveness across various hardware and scenarios, proving its practicality in real-world applications. Code and dataset available at <https://github.com/sharif-apu/LSD-TFFormer>.

1. Introduction

Low-light photography has gained significant popularity due to its aesthetic appeal and widespread availability of compact handheld devices. However, digital cameras usually suffer quantum inefficiency and increase noise levels in low-light conditions, reducing image quality. These challenges have fueled an unprecedented demand for effective

learning-based SLLIE techniques. Beyond aesthetic enhancement, SLLIE has practical applications across various domains, including surveillance, autonomous systems, and general vision tasks such as image matching and object detection (OD) [37, 59, 62].

Learning-based SLLIE remains a challenging problem due to the scarcity of high-quality training datasets and the difficulty of benchmarking solutions across diverse real-world conditions [17]. Notably, the existing SLLIE datasets [13, 27, 49, 55] are often constrained by controlled environments, limited dynamic settings, and semi-synthetic low-light conditions created using fixed ISO values (e.g., ISO 50, 100 in LSRW [13]). In contrast, real-world low-light imaging involves higher ISO values and faster shutter speeds, leading to significant noise, blur, and color distortions [37, 64]. Current datasets fail to capture these complexities, hindering deep models from effectively generalizing to real-world low-light conditions. As a result, deep models tend to amplify noise, introduce unnatural color shifts, and generate artifacts in challenging scenes, as shown in Fig. 1.

Despite data limitations, recent research has explored different SLLIE [17] approaches. The end-to-end learning-based methods [2, 9, 11, 15, 22, 26, 29, 30, 39, 43, 53] aim to directly map low-light images to well-lit counterparts, often integrating Convolutional Neural Networks (CNNs). Several recent methods leverage transformers [7, 41, 52] to enhance the receptive field of vanilla convolutions for learning spatial information, inspired by advances in image restoration [48, 57, 58]. Contrastly, Retinex-based methods [4, 19, 40, 46, 47, 49, 50, 56, 60–63] incorporate Retinex theory into CNN architectures. Retinex-CNN methods typically decompose RGB images, denoise reflectance, and adjust illumination leveraging separate networks. A few recent methods [4, 33, 35] also explored hybrid models combining CNNs, transformers, and Retinex theory to improve visual reconstruction while performing efficient training. Regrettably, these methods can produce desaturation and brightness inconsistencies similar to Retinex-CNN approaches[35]. In sum, SLLIE is hindered by limited

*Rizwan Ali Naqvi and Radu Timofte are corresponding author



Figure 1. Real-world complex scene enhancement using SLLIE datasets. From left to right: Input, LOL-V1 [49], LOL-V2 [55], LSRW [13], and NTIRE challenge on low-light enhancement (NCLLIE) [27], and the proposed LSD. We trained the proposed TFFormer separately on each dataset to evaluate their performance in handling real-world complex scenarios. The proposed LSD helps the model better understand the scene and enhances low-light inputs, avoiding the noise amplification and visual artifacts seen in existing methods.

datasets and model shortcomings, including noise amplification, artifacts, and color distortions in real-world conditions.

In this paper, we tackle the real-world SLLIE by introducing a large-scale dataset and a novel deep network. Our low-light smartphone dataset (**LSD**) comprises 6,425 high-resolution, focus-aligned low-light images with corresponding ground truth. We captured all scenes leveraging dynamic settings and lighting conditions ranging from 0.1 to 200 lux. To ensure diversity, we collected indoor and outdoor image pairs featuring noisy and denoised low-light inputs. We extracted 179,694 patches from 6,025 scenes for training and used the remaining 400 scenes for testing. Additionally, for generalizing SLLIE in real-world scenarios, we collected an unpaired benchmarking dataset (denoted as **LSD-U** in later sections) of over 2,100 unique scenes sourced from smartphones, DSLRs, video frames, social media, etc.

We also introduce **TFFormer**, a tuning fork (TF)-shaped Transformer-CNN model [3, 41, 48] to address learning real-world SLLIE. Taking inspiration from human vision [16, 31], our proposed network learns luminance and chrominance separately instead of using Retinex-based reflection-illumination decomposition. Unlike multi-stage Retinex networks, our streamlined single-network architecture offers a more straightforward design while addressing over-enhancing (i.e., brightness, desaturation, etc.) denoising. It also improves independent noise reduction in luminance and chrominance through the LC attribute. To leverage the LC attributes precisely, we introduce a Luminance-Chrominance Cross-Attention Block (LCCAB) to correlate encoded LC attributes for LC fusion and global consistency. Additionally, we introduce a Luminance-Chrominance Guided Refinement Block (LCGRB) to enhance reconstructions further. To ensure perceptually coherent enhancements, we propose a Luminance-Chrominance Perceptual Loss (LCPL) to guide our network toward generating visually plausible results. The proposed TFFormer outperforms the existing methods in real-world complex SLLIE. We generalize our method in

diverse scenarios. Our contributions are as follows:

1. We collected the largest SLLIE dataset using smartphones. The proposed LSD includes 6,425 focus-aligned high-resolution low-light image pairs and an unpaired benchmark of 2,117 unique scenes from diverse sources.
2. We introduced a TFFormer to outperform existing methods in real-world SLLIE. Our proposed network leverages LC priors along with LCCAB, LCGRB, and LCPL to perceive visually plausible images.
3. We generalized and illustrated the practicability of our method across numerous hardware and use cases. Our evaluation included multiple user studies, perceptual comparisons, quantitative comparisons, and impacts on vision tasks.

2. Low-light Smartphone Dataset (LSD)

2.1. SLLIE Datasets

Four real-world paired datasets have been widely used in existing real-world SLLIE: Low-light (LOL) V1 [49], LOL-V2 [55], LSRW [13], and NCLLIE [27]. Table 1 summarizes the characteristics and sample counts of SLLIE datasets. Notably, the existing datasets were collected in controlled environments and used only a limited range of image sensors. Consequently, they lack diversity regarding light variation and noise, as illustrated in Fig. 2. This scarcity of unique scenes and varied benchmarking samples has significantly constrained progress in SLLIE. Our proposed LSD overcomes these limitations by providing a high-quality dataset specifically designed to tackle the challenges associated with real-world SLLIE. As shown in Fig. 2, our LSD incorporates a broader distribution of light intensity and noise characteristics in the input images and their corresponding ground truth, offering a more diverse and realistic representation of real-world low-light scenarios compared to existing datasets.

2.2. Scene acquisition

Scene Setup. Collecting real-world paired data for SLLIE is significantly challenging, especially in obtaining per-

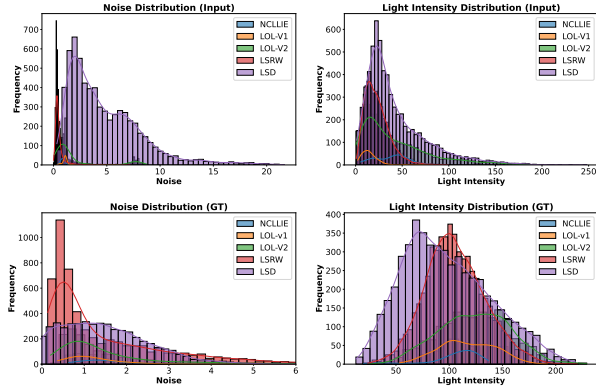


Figure 2. Noise and light intensity distribution comparison between LSD and existing SLLIE datasets. LSD dataset demonstrates higher noise diversity and light intensity variation than existing SLLIE datasets, enhancing SLLIE methods’ generalization.

Dataset	Sensors	ISO	Image Size	Full Scene	Outdoor	Indoor	Training	Testing	Total
LOL-V1 [49]	1	-	400 × 600	✗	36	464	485	15	500
LOL-V2 [55]	1	-	400 × 600	✗	46	743	689	100	789
LSRW [13]	2	50,100	960 × 720	✗	846	4,804	5,600	50	5,650
NCLLIE [27]	1	-	4k+	✓	142	93	210	15	225
LSD	15	50-3200	4k+	✓	3,532	2,893	6,025	400	6,425

Table 1. Details comparison between LSD and SLLIE datasets. The proposed LSD has the most diverse and most number of pair images collected with dynamic settings.

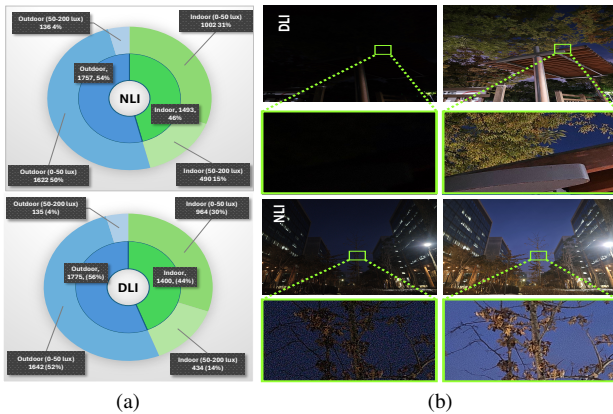


Figure 3. Distribution and sample images of proposed LSD. (a) DLI and NLI distribution, (b) DLI and NLI sample image pairs.

fectly aligned image pairs without motion artifacts or spatial disparity. Despite the challenges, we captured over 8,000 scenes featuring low-light and well-lit reference images. The data was collected in uncontrolled outdoor environments—from sunset to sunrise—using 15 camera setups across six modern smartphones. These smartphones offered diverse camera configurations and allowed for precise control of settings, making them an ideal choice for large-scale data collection. We incorporated a three-frame strategy to ensure spatial alignment, sandwiching each low-light image between two reference images. A proprietary camera app,

developed with the Android Camera API [12], controlled sensitivity, shutter speed, and denoising while other settings remained auto. In each scene, reference images were denoised using the smartphone’s ISP. At the same time, low-light inputs were collected in two versions: (1) Denoised Low-Light Inputs (DLI) and (2) Noisy Low-Light Inputs (NLI), introducing noise diversity. We retained only scenes with at least one perfectly aligned low-light input and reference image, enhancing visibility with histogram matching [36, 38]. Fig. 3b shows sample images from NLI and DLI.

Capture Calibration. We employed a dynamic calibration strategy to capture low-light inputs and their corresponding reference images for introducing dataset’s robustness and diversity. For reference images, settings were calibrated to a low ISO range (i.e., 50–400) to minimize sensor noise. To achieve bright, naturally lit reference images, we used long exposure times, ranging from 1,000 to 15,000 ms, depending on the scene conditions. For low-light inputs, we utilized two distinct capture settings:

1. ISP-driven settings: We took a dummy image in the stock camera app using auto mode before capturing each low-light scene. We then analyzed the sensitivity and shutter speed used in the dummy capture and applied these settings to the low-light input image to replicate camera characteristics.
2. Random-sensitivity settings: ISO and shutter speed configurations are hardware-dependent[20]. However, we aimed to generalize SLLIE across various scenes and devices. Thus, in approximately 60% of scenes, we randomly adjusted ISO and shutter speed to introduce noise diversity while maintaining a low-light scene appearance similar to the dummy capture.

LSD distribution: From over 8,000 collected scenes, we selected 6,425 aligned-focus scenes to construct the LSD dataset, comprising high-resolution image pairs ranging from 3820×2160 to 4080×3060 . The dataset includes 2,893 indoor and 3,532 outdoor scenes captured under diverse lighting conditions from 0.1 to 200 lux, as illustrated in Fig. 3a. We categorized lighting into extreme low-light (0.1–50 lux) and low-light (50–200 lux) conditions. Of these, 6,025 pairs were used for training, while 400 complete scenes were selected for benchmarking, including DLI and NLI samples across various lighting conditions in both indoor and outdoor settings. Further details are provided in the **supplementary** material

2.3. Refining Training Pairs

Despite dynamic settings in uncontrolled environments, reference images may exhibit minor imaging limitations, such as defocus blur, absolute dark regions, and overexposed light sources [20, 24] in localized areas. These issues can occasionally cause deep models to produce blurry regions and inconsistent exposure in extreme cases (see Sec. 4.4).

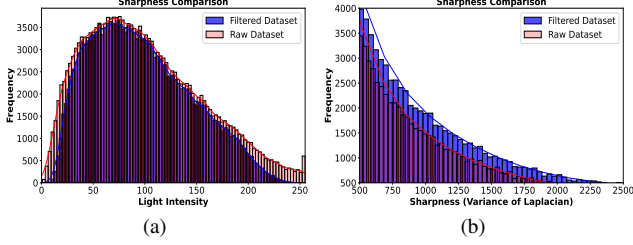


Figure 4. Distribution comparison between filtered and raw training images. (a) intensity filtering. (b) sharpness improvement (blur mitigation).

To mitigate this, we cropped non-overlapping patches of size 512×512 from the reference and low-light images, yielding 208,853 unique training pairs. We eliminated approximately 14% of imperfect pairs by observing the characteristics of the reference images, resulting in 179,695 refined pair patches for learning effective SLLIE. Specifically, the pairs whose reference images have an average brightness below a threshold were discarded. The average brightness I_{avg} of a reference image is calculated as:

$$I_{\text{avg}} = \frac{1}{N} \sum_{i=1}^N I_i \quad \text{where} \quad I_{\text{avg}} < T = 10 \quad (1)$$

where N is the total number of pixels in the image and I_i is the intensity of the i -th pixel.

Additionally, we developed a VGG-based [25] scene classifier to identify and exclude imperfect pairs. The confidence score C for each reference image, computed as $C = f(\mathbf{I}_G)$ (where \mathbf{I}_G represents the reference image), was used to filter out pairs with $C < 0.90$. Since reference images guide deep models in generating plausible outputs, we prioritized their quality during filtering. We also visually inspected the discarded patches to ensure no valuable pairs were lost. Fig. 4 compares the distributions of the raw and filtered patches, highlighting the improvements in intensity and sharpness in the refined training set.

2.4. LSD-U: Unpair Benchmarking Dataset

SLLIE is inherently a matter of aesthetic evaluation, requiring methods to generalize effectively across real-world scenarios. Therefore, the evaluation should involve diverse scenes with a broad distribution rather than relying on datasets with specific biases. To support a comprehensive subjective evaluation in SLLIE, we introduced the LSD-U, including 2,117 unique unpaired test cases. Our benchmark features data from DSLR cameras, smartphones, low-light video frames, and social media images sourced from various users with different photographic styles and setups compared to the proposed LSD. The LSD-U distribution introduces varied biases, enabling SLLIE methods to be tested across a wide range of real-world conditions, including enhancing trillions of social media images.

3. Learning with TFFormer

TFFormer maps a low-light image (\mathbf{I}_{LL}) to an intermediate reconstruction (\mathbf{I}_{rec}) and a refined output (\mathbf{I}_{ref}) as $T : \mathbf{I}_{\text{LL}} \rightarrow \mathbf{I}_{\text{rec}}, \mathbf{I}_{\text{ref}}$. Therefore, we first separated LC and encoded them with a dedicated encoder. The encoded LC features are correlated to capture their dependencies. These encoded-refined features are later decoded to generate an intermediate reconstructed image (\mathbf{I}_{rec}). We refined \mathbf{I}_{rec} further to produce \mathbf{I}_{ref} leveraging LCGRB. Fig. 5 illustrates the overview of the proposed TFFormer.

3.1. Luminance-Chrominance Mapping

We calculated luminance (\mathbf{I}_L) and chrominance prior (\mathbf{I}_C) directly from a given low light image $\mathbf{I}_{\text{LL}} \in \mathbb{R}^{H \times W \times 3}$. Hence, we extracted \mathbf{I}_L leveraging weighted combination of color components [23, 65] and separated \mathbf{I}_C from \mathbf{I}_{LL} as $\mathbf{I}_C = \mathbf{I}_{\text{LL}} - \mathbf{I}_L$. Notably, directly incorporating \mathbf{I}_L into the network enhances fine details and prevents over-brightening, while learning \mathbf{I}_C preserves natural color fidelity and avoids desaturation. Additionally, this separation helps to target noise reduction independently in the structure (luminance) and color (chrominance) components. Therefore, we mapped \mathbf{I}_L and \mathbf{I}_C through mapping function $\text{LC}_{\text{mapping}}$, comprising consecutive *conv* operation (please see 5 (b, c)) to extract features as follows:

$$\mathbf{F}_L, \mathbf{I}_{B_L} = \text{LC}_{\text{mapping}}(\mathbf{I}_{\text{LL}}, \mathbf{I}_L) \quad (2)$$

where $\mathbf{F}_L, \mathbf{I}_{B_L} \in \mathbb{R}^{H \times W \times 40}$ are luminance feature and luminance boosted image (i.e., lit-up image [4]). Similarly, we obtain chrominance feature \mathbf{F}_C and chrominance boosted image \mathbf{I}_{B_C} stated in the above en. 2. Notably, the previous SLLIE method [4] based on Retinex theory calculated boosted image \mathbf{I}_B with illumination features. We found that such direct manipulation utilizing illumination prior pushes the deep networks to focus on the luminance information, ignoring the important chrominance attributes and being prone to over-enhancement.

3.2. LC Encoder-Decoder

The proposed **TFFormer** encodes LC attributes using the dedicated encoder. The luminance encoder learns to map $\{\mathbf{I}_{B_L}, \mathbf{F}_L\}$ as $\{\mathbf{I}_{B_L}^*, \mathbf{F}_L^*\} = \mathbf{E}_L \in \mathbb{R}^{(\frac{H}{8}) \times (\frac{W}{8}) \times 320}$. Similarly, we obtain chrominance encoder features as $\{\mathbf{I}_{B_C}^*, \mathbf{F}_C^*\} = \mathbf{E}_C \in \mathbb{R}^{(\frac{H}{8}) \times (\frac{W}{8}) \times 320}$. We refined the encoded LC features further, leveraging our proposed cross-attention module (sec. 3.3) for inter-attribute correlation to generate \mathbf{A}_{LC} . We combine correlated feature (\mathbf{A}_{LC}) along with \mathbf{E}_L and \mathbf{E}_C to reconstruct an intermediate image $\mathbf{I}_{\text{rec}} \in \mathbb{R}^{H \times W \times 3}$. To leverage LC properties and salient feature extraction effectively, we introduce LCGAB (an extension of IGAB [4]) in the encoder-decoder blocks (see Fig. 5).

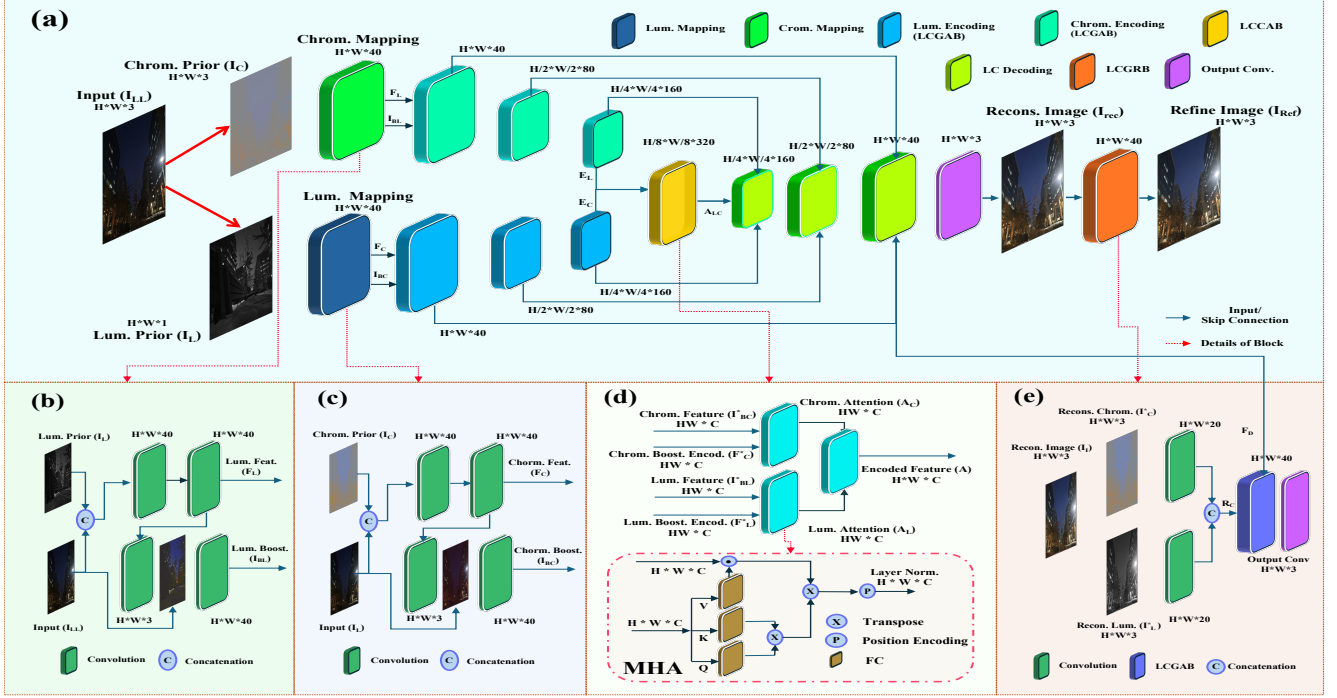


Figure 5. Overview of proposed TFFormer. (a) Overall architecture, (b) Chrominance mapping, (c) Luminance mapping, (d) LCCAB, and (e) LCGRB.

3.3. LC Cross Attention Block (LCCAB)

We leverage LCCAB to refine and correlate luminance and chrominance features. Therefore, we leverage multihead self-attention (S) [4, 45, 48, 52] to refine encoded (E_L) and (E_C) features such as $A_L = S(E_L)$ and $A_C = S(E_C)$. Here $(A_L, A_C) \in \mathbb{R}^{HW \times 320}$. We further refined and correlated the luminance attention A_L and chrominance attention A_C with multi-head cross-attention (CA) block to enhance inter-domain correlation and capture global attention over LC encoding as:

$$A_{LC} = CA(A_L, A_C) = \text{softmax} \left(\frac{QK^T}{\sqrt{d_k}} \right) V, \quad (3)$$

Here $(A_L, A_C) \in \mathbb{R}^{HW \times C}$ is further split into k heads such that $(A_L, A_C) \in \mathbb{R}^{HW \times d_k}$, $d_k = \frac{C}{k}$ where $k=8$. Q, K, V are projections of A_L and A_C into query, key, and value spaces. Here, LC cross-attention captures long-range dependencies between the luminance and chrominance domains, improving global illumination and color constancy during the reconstruction of I_{rec} .

3.4. LC Guided Reconstruction Block (LCGRB)

The proposed LCGRB refine the intermediate image as $R : I_{LRec} \rightarrow I_{Ref}$. Therefore, it extract the reconstructed luminance (I_L^*) and reconstructed chrominance (I_C^*) (similar to Sec. 3.1) and map them as $I_L^* \in \mathbb{R}^{H \times W \times 20}$ and $I_C^* \in \mathbb{R}^{H \times W \times 20}$. We leverage $conv_{3 \times 3}$ for high-dimensional projections of LC properties to map combined

feature $R_C \in \mathbb{R}^{H \times W \times 40}$. We feed R_C and decoded feature $F_D \in \mathbb{R}^{H \times W \times 40}$ to LCGAB to obtain the refined output (I_{ref}), as shown in Fig. 5 (d). LCGRB helps TFFormer to refine its reconstructions globally by leveraging LC properties without introducing any further training phase.

3.5. LC Perceptual Loss (LCPL)

The core idea of TFFormer is to leverage LC attributes within a deep network. To enhance alignment and refinement, we compute per-pixel LC distance by comparing ground truth and generated LC components. Our proposed LCPL enforces consistency between intermediate and refined representations, improving color fidelity and structural details. The per-pixel LC distance is defined as:

$$D_{LC} = \frac{1}{N} \sum_{i=1}^N \left(\|I_{G,L}^{(i)} - I_{rec,L}^{(i)}\|_1 + \|I_{G,C}^{(i)} - I_{rec,C}^{(i)}\|_1 \right) \quad (4)$$

where $I_{G,L}$ and $I_{rec,L}$ represent the luminance components of the ground truth and reconstructed images, respectively. $I_{G,C}$ and $I_{rec,C}$ represent the chrominance components. N is the total number of pixels. The LC loss is formulated to guide the network in learning LC representations effectively:

$$\mathcal{L}_{LC} = D_{LC}(I_G, I_{rec}) + D_{LC}(I_G, I_{ref}) \quad (5)$$

We leverage I_{ref} and I_{rec} images to calculate our perceptual loss, enhance gradient flow, stabilize training, and enable progressive refinement for improved performance.

Model	Type	Low-light						Extreme Low-light						LSD		
		Indoor			Outdoor			Indoor			Outdoor			Average		
		PSNR \uparrow	SSIM \uparrow	LPIPS \downarrow	PSNR \uparrow	SSIM \uparrow	LPIPS \downarrow	PSNR \uparrow	SSIM \uparrow	LPIPS \downarrow	PSNR \uparrow	SSIM \uparrow	LPIPS \downarrow	PSNR \uparrow	SSIM \uparrow	LPIPS \downarrow
Retinexnet [49]		14.57	0.6327	0.2611	13.70	0.5489	0.3150	15.63	0.5754	0.3064	14.34	0.4871	0.3875	14.56	0.5610	0.3175
Kind [61]		13.55	0.6717	0.2665	13.47	0.6287	0.3174	14.21	0.6320	0.3001	13.25	0.6047	0.3521	13.62	0.6343	0.3090
Kind+ [62]		13.49	0.6630	0.2871	13.17	0.6138	0.3411	13.94	0.6141	0.3275	13.13	0.5899	0.3733	13.43	0.6202	0.3322
DeepUPE [47]		15.73	0.5874	0.3008	15.03	0.5620	0.2841	14.99	0.4612	0.4104	16.30	0.4378	0.4131	15.51	0.5121	0.3521
SNRNet [52]	DLI	15.14	0.6326	0.3776	14.82	0.3510	0.7161	13.05	0.5377	0.4450	15.43	0.4646	0.5720	14.61	0.4965	0.5277
MIRNet [57]		16.15	0.7206	0.2284	14.01	0.5600	0.3632	15.51	0.6360	0.2700	17.20	0.5811	0.3085	15.72	0.6244	0.2925
Uformer [48]		13.04	0.6578	0.2672	12.40	0.5423	0.3635	11.93	0.5575	0.3092	13.46	0.5006	0.3593	12.71	0.5646	0.3248
IAT [7]		13.34	0.6557	0.2819	13.31	0.4680	0.4320	14.82	0.4978	0.3944	13.07	0.5600	0.3583	13.64	0.5454	0.3667
Retinexformer [4]		17.77	0.7338	0.2138	17.40	0.5828	0.3199	17.53	0.6591	0.2545	17.40	0.5828	0.3199	17.53	0.6396	0.2770
TFFormer		19.99	0.7620	0.2129	17.72	0.6830	0.2557	18.86	0.7121	0.2430	19.95	0.6555	0.3124	19.13	0.7031	0.2560
Retinexnet [49]		14.11	0.5456	0.3465	13.21	0.5234	0.3710	14.44	0.4252	0.5545	13.50	0.4078	0.5077	13.81	0.4755	0.4449
Kind [61]		13.49	0.5330	0.3495	13.09	0.5701	0.3280	13.43	0.4331	0.4819	13.13	0.5532	0.3699	13.28	0.5223	0.3823
Kind+ [62]		13.22	0.5283	0.3662	12.70	0.5667	0.3405	13.62	0.4214	0.4949	12.90	0.4476	0.4625	13.11	0.4910	0.4160
DeepUPE [47]		14.11	0.3529	0.5667	13.42	0.4061	0.4229	12.79	0.2125	0.7857	14.01	0.2799	0.6351	13.58	0.3128	0.6026
SNRNet [52]	NLI	16.66	0.5793	0.4208	14.95	0.3025	0.7497	14.04	0.4882	0.5207	16.60	0.4110	0.6183	15.56	0.4453	0.5774
MIRNet [57]		14.82	0.6551	0.2523	13.64	0.5297	0.3274	12.80	0.5291	0.3615	16.74	0.5524	0.3300	14.50	0.5666	0.3178
Uformer [48]		13.85	0.6570	0.2628	13.07	0.5654	0.3315	12.53	0.5591	0.3488	14.13	0.5325	0.3609	13.39	0.5785	0.3260
IAT [7]		15.35	0.6506	0.2612	13.92	0.5248	0.3434	13.33	0.5308	0.3980	15.88	0.5062	0.3671	14.62	0.5531	0.3424
Retinexformer [4]		18.00	0.6934	0.2470	14.99	0.5531	0.3534	17.47	0.6094	0.3387	17.89	0.5822	0.3564	17.08	0.6095	0.3239
TFFormer		19.34	0.7198	0.2445	17.91	0.6837	0.2394	19.27	0.6923	0.3048	20.34	0.6401	0.3034	19.21	0.6840	0.2730

Table 2. Quantitative comparison of SLLIE methods on proposed LSD. Our proposed TFFormer outperforms the existing methods by a notable margin. The best and the second-best results are highlighted in red and blue, respectively. Best viewed in zoom.

4. Experiments

4.1. Comparison between SLLIE methods

We evaluated state-of-the-art (SOTA) methods to summarize their performance on real SLLIE. This study focused on Retinex-based models, including RetinexNet [49], Kind [61], Kind+ [62], and DeepUPE [47], as well as transformer-based SLLIE methods like Retinexformer [4], IAT [7], and SNRNet [52]. We also assessed the capabilities of SOTA restoration models, Uformer [48], and MIRNet [57], to evaluate their applicability in real-world SLLIE scenarios. Please note that we included methods that leverage Retinex theory or transformer architectures for fair comparison. We verified the reported results from their respective papers through our implementations using the recommended datasets before training them with the proposed LSD. To further generalize our findings, we trained all models on a combined dataset comprising both DLI and NLI images, ensuring a robust evaluation across diverse real-world conditions.

Quantitative Evaluation. Tab. 2 presents the performance of our SLLIE methods on the LSD dataset, covering both indoor and outdoor scenes captured under low-light and extreme low-light conditions. Our evaluation demonstrates that the proposed TFFormer consistently outperforms SOTA methods under all conditions, including denoised (DLI) and noisy (NLI) scenarios. In comparison to the most substantial baseline, RetinexFormer [4], TFFormer delivers improvements of **1.6 dB** in PSNR, **0.0635** in SSIM, and a reduction of **0.021** in LPIPS on the DLI subset, as well as gains of **2.13 dB** in PSNR, **0.0745** in SSIM, and a reduction of **0.0509** in LPIPS on the NLI subset. On average, TFFormer achieves enhancements of **1.865 dB** in PSNR, **0.138** in SSIM, and a decrease of **0.0719** in LPIPS, high-

lighting its superior performance across diverse real-world low-light conditions.

Qualitative Evaluation. Fig. 6 visually confirms the performance and drawbacks of the SLLIE methods on our LSD. Our model can generate visually plausible results with consistent brightness, better denoising, and less visible artifacts. Also, with and without noise, our TFFormer illustrates a consistent performance for enhancing complex low-light scenes.

4.2. Cross-dataset Evaluation

4.2.1. Perceptual Comparison

The proposed LSD is designed to handle diverse real-world low-light scenarios effectively. We conducted the cross-dataset comparison to assess its practical applicability and user acceptance, evaluating enhancement results from both existing SLLIE datasets and our proposed LSD. Notably, LSD-U was collected independently of LSD to ensure an unbiased evaluation. Our cross-dataset evaluation aims to provide a fair and comprehensive comparison of SLLIE datasets rather than assessing performance on dataset-specific training distributions. Therefore, we trained our TFFormer model on SLLIE datasets and our LSD dataset. To evaluate model generalization on unknown, real-world scenes captured by various hardware, we conducted an extensive perceptual comparison and user study using our collected LSD-U benchmarking dataset. For this study, we invited **15** participants, each reviewing **5 out of 2,117** randomly selected image sets, ranking the images based on personal preference. We summarized these rankings using the Bradley-Terry model [1] to demonstrate model practicality for real-world SLLIE. As illustrated in Fig. 7, user preferences and perceptual comparisons indi-

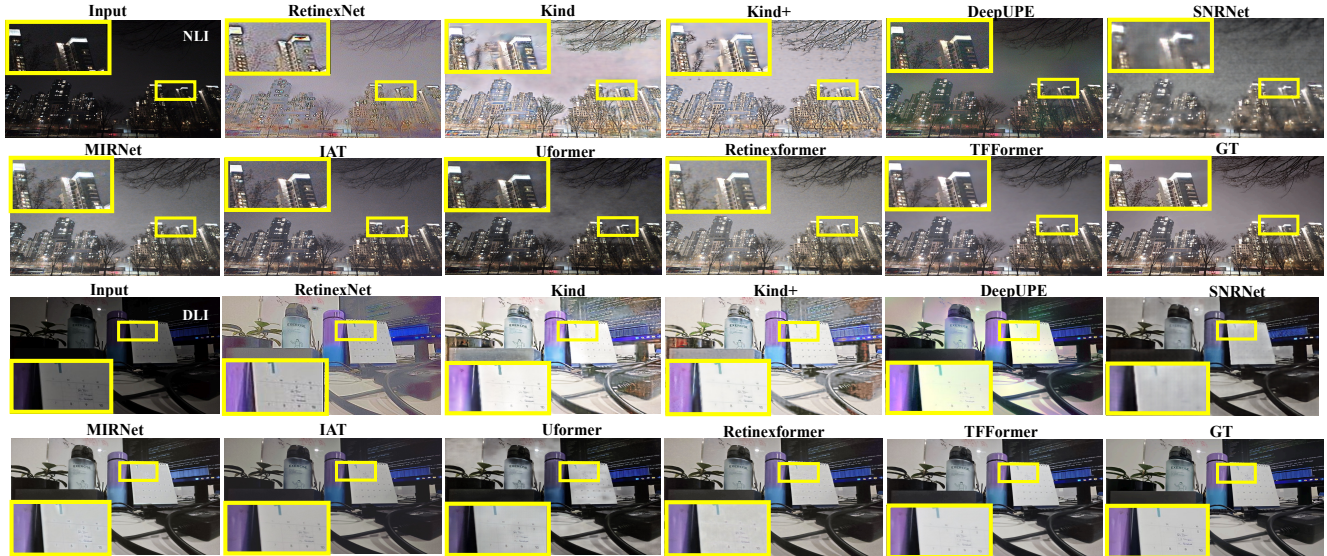


Figure 6. Qualitative comparison of existing SLLIE methods on the LSD dataset. The top scenes show performance on NLI, while the bottom examples illustrate performance on DLI scene types. TFFormer produces cleaner-plausible images, outperforming existing methods..

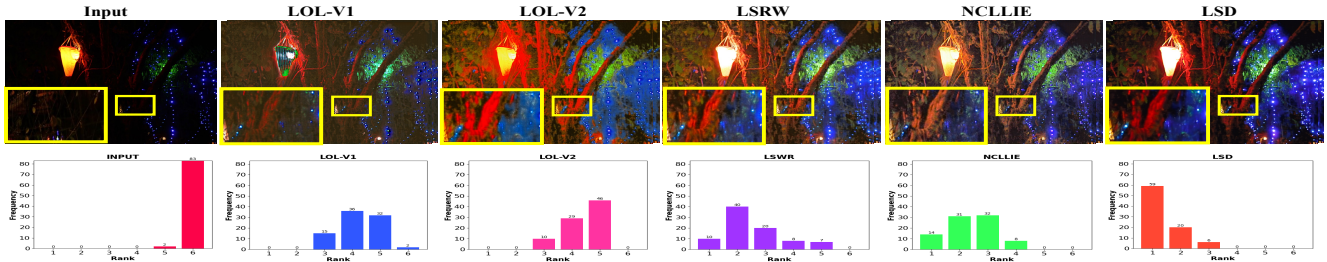


Figure 7. Cross-dataset evaluation on LSD-U. Top row: low-light image enhanced by SLLIE dataset, bottom row: user rank of performance of the SLLIE method summarized by bredly-terry model.

cate that our proposed method consistently outperformed the method trained on the existing SLLIE dataset.

Dataset/Class	Bicycle	Boat	Bottle	Bus	Car	Cat	Chair	Cup	Dog	Motorbike	People	Table	mAP
ExDark [28]	43.10	27.50	28.30	60.70	42.70	25.60	21.90	32.30	29.60	21.40	29.00	21.70	32.00
LOL-V1 [49]	56.00	29.70	35.50	63.50	46.70	36.90	31.10	30.60	38.80	23.40	35.60	27.50	37.90
LOL-V2 [55]	48.40	27.00	27.50	60.20	40.60	33.30	31.20	27.10	35.30	19.50	32.20	30.20	34.40
LSRW [13]	59.10	31.80	36.50	63.60	43.90	34.40	29.00	23.50	31.70	16.40	32.50	29.10	35.90
NCLLIE [27]	51.90	31.40	33.60	62.60	44.20	38.50	31.70	29.50	34.00	20.80	33.90	30.00	36.80
LSD	54.00	31.00	35.30	61.80	47.80	40.50	33.10	32.50	39.70	24.20	36.20	30.00	38.80

Table 3. Object-detection on low-light scenarios. The proposed LSD can enhance the visibility and details of low-light images, resulting in significant detection improvement. The best and the second-best results are highlighted in red and blue, respectively.

4.2.2. Vision Tasks

In addition to the visual enhancement, a robust SLLIE dataset can enhance vision tasks under stochastic lighting conditions. To assess the effectiveness of our LSD, we applied it alongside other SLLIE datasets to enhance the ExDark [28] validation dataset comprising 1,473 images and 13 object classes. We then evaluated object detection per-

formance using the YOLOv3 model [10], trained on the COCO dataset. Tab. 3 shows that the proposed LSD improves detection accuracy by **6.80** mAP compared to the low-light ExDark inputs, outperforming other datasets.

4.3. Generalization across devices

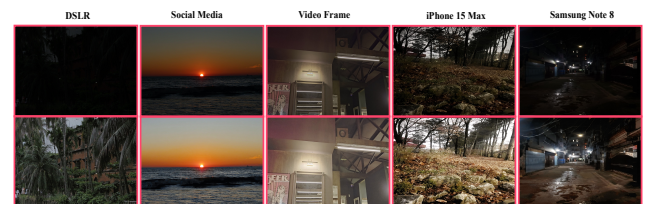


Figure 8. Performance of LSD-TFFormer on diverse sources. Our method can enhance old social media images from eight years ago, even if they are heavily compressed. Best viewed in zoom.

Fig. 8 shows the performance of LSD-TFFormer across various scenarios. Despite being trained on single-shot im-

ages, our model adapts well to video frames and can enhance photos taken on older devices, such as the eight-year-old Samsung Note 8. LSD-TFFormer can also effectively revive decade-old compressed images from social media images without visible artifacts. A separate user study confirmed the real-world effectiveness of the proposed method, with over **82%** of participants preferring the enhanced images over their low-light counterparts. Please refer to the **supplementary materials** for more details.

4.4. Ablation Study

Scene Type	DLI			NLI			LSD (Average)		
	PSNR \uparrow	SSIM \uparrow	LPIPS \downarrow	PSNR \uparrow	SSIM \uparrow	LPIPS \downarrow	PSNR \uparrow	SSIM \uparrow	LPIPS \downarrow
Raw Patch	15.47	0.6330	0.3107	15.80	0.6293	0.3155	15.64	0.6312	0.3131
Full-scene	17.52	0.6396	0.2770	17.09	0.6095	0.3239	17.31	0.6246	0.3005
Filtered Patch	19.13	0.7024	0.2553	19.21	0.6840	0.2730	19.17	0.6932	0.2641

Table 4. Ablation study on LSD. The proposed filtered patches help the deep model to produce more natural-looking enhanced images. The best and the second-best results are highlighted in **red** and **blue**.

LSD. Fig. 9 shows TFFormer’s performance with filter patch training, full-scene training, and raw patch training. Our selective patch training approach allows TFFormer to learn local noise patterns better, preserving fine details in complex areas. In contrast, non-selective training often produces blurry outputs due to motion blur in the GT images, while full-scene training limits the model’s focus on intricate noise, emphasizing global attributes. Tab. 4 summarizes TFFormer’s performance on LSD (training) variants. Compared to the full-scene training, filter patches can improve TFFormer performance by **2.14** dB on PSNR.

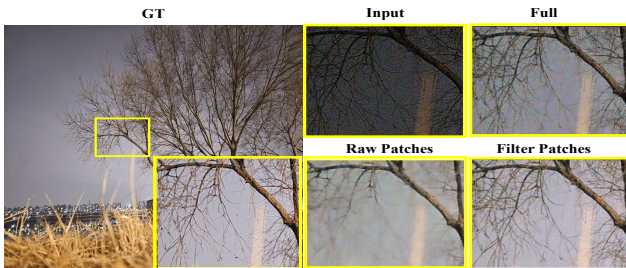


Figure 9. Ablation study on LSD, patch and full-scene training

TFFormer In our ablation study, we evaluated each novel component of TFFormer by starting with a base model and progressively adding LCE, LCCAB, LCGRB, and LCPL. The LCE variant enhances denoising and color consistency, LCCAB improves feature correlation for global reconstruction, LCGRB refines the projected intermediate outputs, and LCP loss enhances the perceptual quality of the reconstructed image. TFFormer achieves the best results by combining all components, as shown in Tab. 5. Fig. 10 further confirms the contribution of the proposed component by visual comparison.

Module				DLI		NLI		LSD (Average)				
LCE	LCCAB	LCGRB	LCPL	PSNR \uparrow	SSIM \uparrow	PSNR \uparrow	SSIM \uparrow	PSNR \uparrow	SSIM \uparrow	LPIPS \downarrow		
X	X	X	X	15.46	0.6248	0.2856	15.27	0.5942	0.2949	15.36	0.6095	0.2903
X	X	X	X	16.65	0.6469	0.2817	16.82	0.6265	0.2775	16.74	0.6367	0.2796
X	X	X	X	17.66	0.6805	0.2783	17.87	0.6506	0.2728	17.77	0.6656	0.2756
X	X	X	X	17.74	0.6856	0.2706	17.99	0.6697	0.2840	17.86	0.6776	0.2773
X	X	X	X	19.13	0.7024	0.2553	19.21	0.6849	0.2730	19.17	0.6932	0.2641

Table 5. Ablation study on TFFormer. The proposed component helps the TFFormer in achieving SOTA performance on LSD. The best and the second-best results are highlighted in **red** and **blue**.



Figure 10. Ablation study on the novel component of proposed TFFormer on LSD.

4.5. Discussion

The proposed method illustrates the practicability of a generic SLLIE method. Also, it reveals the limitations of existing SLLIE datasets and models. Please refer to the **supplementary material** for more details and results. Despite promising results, we observed that all deep models, including TFFormer, could struggle to produce visually appealing images in some extreme cases (e.g., NLI capture under 1 lux). Therefore, it has been planned that extreme low-light NLI enhancement will be studied separately through a future study. Also, joint OD with SLLIE could be an exciting choice for many industry applications.

5. Conclusion

This study proposed the largest SLLIE dataset collected with numerous hardware and sources. Our proposed LSD dataset contains 6,425 high-resolution low-light images with corresponding reference images. We collected these image pairs using dynamic calibration settings tailored to each device and capture condition. From these, we utilized 6,025 pairs to generate approximately 180,000 refined training patches and reserved an additional 400 full-scene images for SLLIE benchmarking. Furthermore, we collected 2,117 unique low-light scenes from diverse sources for aesthetic evaluations. Additionally, we proposed a novel deep model to learn SLLIE from collected data samples. Our proposed model leverages LC attributes in the transformer model to maintain color accuracy while denoising. We also incorporated an LCCAB, LCGRB, and LCPL to accelerate our SLLIE performance. We generalized our model for numerous hardware and extensively evaluated its practicability. It has been planned to learn joint SLLIE-OD and extreme NLI enhancement through a future study.

Supplementary Material

This supplementary document details the LSD preparation and insights of TFFormer, provides additional experimental results, and discusses the limitations of the proposed method. We organized the document as follows:

- Section A details LSD preparation
- Section B details the distribution of the LSD and illustrates the limitation of the existing dataset visually.
- Section C provides learning details and performance of the TFFormer in existing SLLIE.
- Section D provides additional experimental results

A. LSD Preparation

We designed our LSD app carefully to collect a large-scale SLLIE dataset leveraging multiple sensors for diverse real-world data collection. We also developed our scene classifier by utilizing the capability of SOTA image classification models.

A.1. Sensor Details

To diversify our proposed LSD dataset, we utilize 15 distinct image sensors from six different smartphones, encompassing a variety of imaging principles, resolutions, pixel sizes, and sensor sizes. These sensors respond uniquely to various lighting conditions, particularly noise, dynamic range, and color reproduction. Table 6 provides the specifications of these smartphones and their cameras, with the resolution reflecting the maximum native output of each sensor. However, under low-light conditions, these sensors typically generate 4K images by leveraging pixel-binning techniques to create larger effective pixels, enhancing brightness and reducing noise.

This study replicates real-world scenarios using the default pixel-binning configurations of modern smartphones. Only the rear cameras were employed, as they offer superior imaging performance compared to front-facing cameras. The diversity in sensor types, field of view, and imaging characteristics substantially enriches the LSD dataset, ensuring its robustness and relevance for low-light image enhancement research.

A.2. LSD App

Our LSD app was developed by leveraging android-api [12] to capture aligned low-light and corresponding reference images. Before fixing the final version, we experimented with the available APIs to find the best and easy-to-use interface for collecting low-light samples. Fig. 11 illustrates the sample screenshot of our LSD app. To capture a scene, we first selected a random camera sensor for the device; we calibrated the settings based on our capture calibration strategy. Before saving the scenes, we visually inspected the captured scenes to ensure their usability.

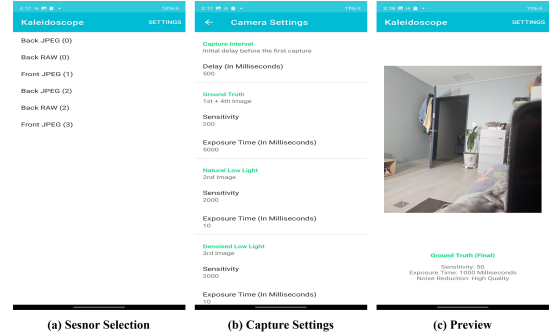


Figure 11. User interface and detail of LSD APP. (a) Selecting Sensor. (b) Settings adjustment of low-light and reference images. (c) Preview of capture scenes

A.3. VGGScene Classifier

Refining the collected patches from our image pairs posed significant challenges, mainly due to unwanted imaging limitations such as blurs, over-exposed light sources, dark under-exposed regions, and defocus in reference images. Developing individual algorithms to address each issue proved inefficient and complex, while manually inspecting every image pair was impractical.

To overcome these hurdles, we developed a learning-based scene classifier to automate and accelerate the refinement process. This approach enabled us to identify and exclude imperfect images from training, ensuring higher dataset quality. Before beginning the LSD scene collection, we extensively evaluated state-of-the-art (SOTA) classification methods and constructed a separate scene classification dataset to fine-tune our classifier. This allowed us to handle challenging scenarios and streamline the refinement process robustly.

A.3.1. Data Preparation.

Before start collecting the LSD dataset, we captured around 200 random scenes to find the limitations and probable obstacles of preprocessing our LSD. Also, we made a list of unwanted imaging consequences that may affect our learning strategy. Based on the initial study, we made a classification dataset and separated perfect and imperfect scenes into two categories. Tab. 7 illustrates the detail of our scene classification dataset. We collected 12,770 image patches to learn scene classifiers with SOTA classification methods. Fig. 12 demonstrates the sample images from our scene classification dataset.

A.3.2. Experiments and Results.

We studied the existing classification method to learn the perfect scene identification. We alter the final classification layer of SOTA models to fit our objective [42]. Additionally, we leverage Imagenet’s [8] pre-trained weights of these methods from the torch-vision [6] library to acceler-

Device	Camera	Sensor	Resolution (Max.)	Sensor Size	Pixel Size	Aperture	Year
Samsung Galaxy S10	Main (Wide)	S5K2L4	12 MP (4032 x 3024)	1/2.55 in.	1.4 μm	f/1.5-2.4	2019
	Telephoto	S5K3M3	12 MP (4032 x 3024)	1/3.6 in.	1.0 μm	f/2.4	2019
	Ultra-Wide	S5K4H5	16 MP (4608 x 3456)	1/3.1 in.	1.0 μm	f/2.2	2019
Samsung Galaxy Z Flip3	Main (Wide)	IMX555	12 MP (4032 x 3024)	1/2.55 in.	1.4 μm	f/1.8	2021
	Ultra-Wide	IMX258	12 MP (4000 x 3000)	1/3.0 in.	1.12 μm	f/2.2	2021
Xiaomi Redmi 10C	Main (Wide)	ISOCELL JN1	50 MP (8160 x 6144)	1/2.76 in.	0.64 μm	f/1.8	2022
Samsung Galaxy S22 Ultra	Main (Wide)	HM3	108 MP (12032 x 9024)	1/1.33 in.	0.8 μm	f/1.8	2022
	Telephoto (3x)	IMX754	10 MP (3648 x 2736)	1/3.52 in.	1.12 μm	f/2.4	2022
	Telephoto (10x)	IMX754	10 MP (3648 x 2736)	1/3.52 in.	1.12 μm	f/4.9	2022
	Ultra-Wide	IMX563	12 MP (4000 x 3000)	1/2.55 in.	1.4 μm	f/2.2	2022
Samsung Galaxy Z Flip5	Main (Wide)	IMX563	12 MP (4032 x 3024)	1/1.76 in.	1.8 μm	f/1.8	2023
	Ultra-Wide	IMX258	12 MP (4000 x 3000)	1/2.55 in.	1.12 μm	f/2.2	2023
Samsung Galaxy Z Fold5	Main (Wide)	GN5	50 MP (8160 x 6120)	1/1.57 in.	1.0 μm	f/1.8	2023
	Telephoto	IMX754	10 MP (3648 x 2736)	1/3.94 in.	1.0 μm	f/2.4	2023
	Ultra-Wide	IMX563	12 MP (4000 x 3000)	1/3.0 in.	1.12 μm	f/2.2	2023

Table 6. Specifications of the camera sensors utilized to collect the proposed LSD. Utilizing such diverse sensors helps us generalize the SLLIE in the real world for practical use.



Figure 12. Sample images from scene classification dataset. (a) Imperfect scenes. (b) Perfect scenes.

Class	Train	Test
Perfect	5,580	755
Imperfect	5,456	979
Total	11,036	1,734

Table 7. Detail of LSD scene classification dataset.

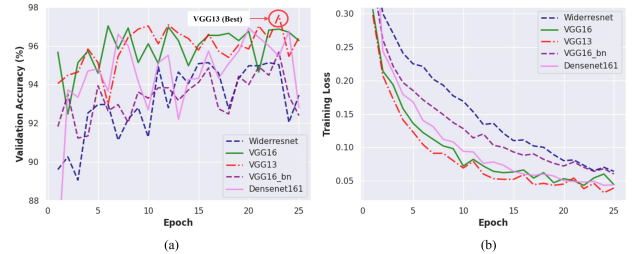


Figure 13. Learning scene classification with SOTA image classification methods. (a) Validation accuracy vs epoch. (b) Training loss vs epoch.

ate the learning process and achieve faster convergence. We trained existing methods for 25 epochs with their suggested hyperparameters. Fig. 13 details the training loss and validation accuracy of the SOTA classification method on LSD scene classification. VGG13 [25] illustrates the maximum validation accuracy among the SOTA classification methods. Based on the experimental results, we leverage the best weight of VGG13 for making our LSD scene classifier. Tab. 8 compares numerous deep methods in LSD scene classification.

Fig. 14 illustrates the sample images eliminated by our patch filtering strategy.

Model	Accuracy (%)
Widerresnet [51]	95.13
VGG16 [25]	97.02
VGG16_bn [25]	95.67
Densenet161 [14]	96.92
VGG13 [25]	97.57

Table 8. Comparison between SOTA deep image classification methods on LSD scene classification.

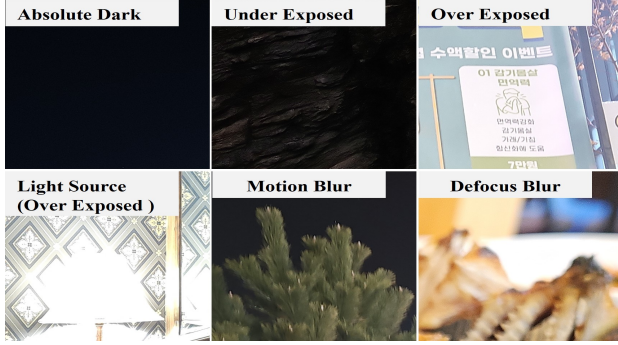


Figure 14. Sample images were eliminated through our patch filtering strategy.

B. LSD vs. Existing Datasets

B.1. Training Scenes

Capturing images in real-world, uncontrolled environments offers significant advantages, particularly in replicating scenarios where images are taken with handheld cameras. However, such conditions often introduce imaging limitations, such as blurs, over-exposed highlights, and under-exposed regions, especially in the reference images. These imperfections can mislead deep learning models and result in unusable outputs.

To address this, we refined our training dataset by filtering out images with these limitations. This was achieved by analyzing the global intensity of reference images and leveraging our VGG-based scene classifier for robust filtering. Tab .9 provides a detailed breakdown of the device-wise distribution of the refined LSD training dataset, highlighting the diversity and quality ensured through this process. It is worth noting that some devices may use the same image sensor. However, these setups employ different focal lengths and image processing techniques, ensuring that the resulting samples remain diverse even when the same sensor is utilized.

B.2. Testing Scenes

One major limitation of the current SLLIE datasets is the absence of diverse testing scenes. To counter this, we curated the most extensive benchmarking test set, incorporating a variety of hardware, scenes, and sources. Tab. 10 details our LSD test set. For comprehensive evaluation, our test set includes paired scenes for quantitative and qualitative assessments and unpaired images for subjective evaluation.

B.2.1. Pair Images.

We collected 400 testing scenes for pair testing, including DLL and NLL pairs captured in different lighting conditions. Each of these categories also includes subsets for in-

door and outdoor samples. For testing scenes, we selected the full scenes with minimal unexpected imaging instances.

B.2.2. Unpair Images.

Image enhancement invariably remains debatable, contingent upon personal preferences. Therefore, the proposed LSD offers 2,117 unique test cases for extensive subjective assessment. Our unpaired testing set encompasses data samples captured with DSLR cameras, smartphones, frames from 10 low-light videos, and social media images. We observed millions of images stored on social media, which can still benefit from SLLIE techniques, breathing new life into them.

B.3. Limitation of Existing SLLIE Datasets

Existing SLLIE datasets predominantly consist of scenes captured under well-lit conditions, with low-light inputs artificially generated using low ISO settings and short exposure times. As shown in Fig. 15, these samples are often taken in high-brightness outdoor environments, making the dataset semi-synthesized rather than representative of actual low-light scenarios. While useful for controlled experiments, this approach fails to authentically replicate the challenges faced in natural low-light environments, such as complex lighting distributions, varying noise levels, and diverse low-illumination conditions.

Moreover, these brighter scenes often contain naturally underexposed regions better suited for HDR mapping than developing and evaluating dedicated SLLIE methods. This mismatch can mislead model development, as the dataset does not fully capture the nuanced challenges of real low-light imaging. To advance SLLIE research, it is essential to focus on datasets that authentically represent diverse low-light conditions rather than relying on semi-synthetic approximations.

In contrast to the existing SLLIE datasets, we collected our datasets in actual low-light scenarios (0.1-200 lux). Fig. 16 illustrates the samples from the proposed LSD. We collected data over the years in different seasons, such as winter, autumn, and summer.

C. TFFormer

Due to page limits, our main article could not provide details on implementing TFFormer, LC loss, and complexity analysis. This section details the missing part to ensure the reproducibility of our proposed method.

C.1. Implementation Details

LC Extraction: Luminance-Chrominance (LC) extraction separates an image’s intensity and color information. Luminance (L) is computed as $L = 0.299R + 0.587G + 0.114B$, representing brightness based on human visual perception. Where R, G, and B are color channels of

Device	DLI	NLI	Combine	Raw Patches	Filtered Patches	Usable Patch (%)
Samsung Galaxy S10	84	67	151	5,185	3,847	74.19
Samsung Galaxy Z Fold 5	759	689	1448	56,577	50,416	89.11
Samsung Galaxy S 22 Ultra	1,270	1,420	2,690	85,471	75,514	88.35
Samsung Galaxy Z Flip 3	329	347	676	22,800	20,312	89.09
Xiaomi Redmi 10C	166	161	327	9,163	8,439	92.10
Samsung Galaxy Z Flip5	367	366	733	29,657	21,167	71.37
Total	2,975	3,050	6,025	208,853	179,695	86.04

Table 9. Details of LSD training set (filtered). We filtered out around 15% of patch pairs to make our training set robust.

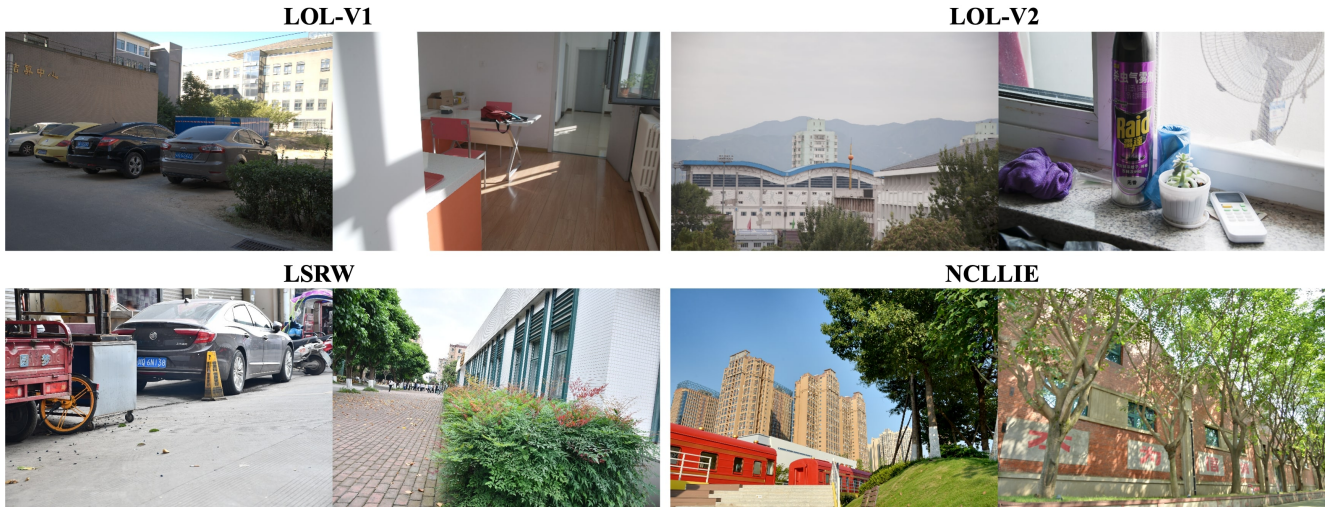


Figure 15. Sample images from existing SLLIE dataset. Many of the collected scenes of these datasets are captured in bright outdoor scenes and replicated in the low-light input by controlling camera parameters.



Figure 16. Sample images LSD. We collected all samples in 0.1-200 lux for over two years. (a) Samples from DLI scenes. (b) Samples from NLI scenes

Type	Lighting Condition	Category	Scenes
Pair	Low-light	DLI	100
	Extreme	DLI	100
	Low-light	NLI	100
	Extreme	NLI	100
Unpair	Mix	Android	300
		iPhone	250
		DSLR	300
		Social Media	50
		Video Frames	1,217
Total			2,517

Table 10. Detail of our LSD benchmarking set. We developed the largest and most diverse SLLIE benchmarking dataset throughout this study.

an image. Chrominance (C) captures color details by subtracting luminance from the original Image: $C = I - L$. This decomposition is widely used in image processing for tasks like compression, enhancement, and object tracking, enabling better independent handling of brightness and color.

LC Encoding: We expanded the luminance-boosted image (\mathbf{I}_{BL}), luminance features (\mathbf{F}_L), chrominance-boosted image (\mathbf{I}_{BC}) and chrominance features (\mathbf{F}_C) into same feature dimension as $\mathbf{F}_x \in \mathbb{R}^{H \times W \times 40}$. Later, we feed our luminance and chrominance encoder with these expanded feature maps to obtain $\mathbf{I}_{L_{enc}}$ or $\mathbf{I}_{C_{enc}}$. Our luminance and chrominance encoders comprise the LCGAB, followed by two convolution operations with stride 2 to down-sample the LC attributes and boosted-image maps. We expanded the dimension of the feature channel by a factor of 2 in every recurring encoder block. Also, we reduced the spatial dimension by a factor of 2 while expanding the feature maps in both encoders to obtain $\mathbf{I}_{BL_{down}}$ and $\mathbf{I}_{FL_{down}}$.

$$\mathbf{I}_{L_{enc}} = LCGAB(\mathbf{I}_{BL}, \mathbf{F}_L) \quad (6)$$

$$\mathbf{I}_{BL_{down}} = Conv(\mathbf{I}_{enc}, s = 2) \quad (7)$$

$$\mathbf{I}_{FL_{down}} = Conv(\mathbf{F}_L, s = 2) \quad (8)$$

The Chrominance branch follows the same equation to obtain their respective images $\mathbf{I}_{C_{enc}}$, $\mathbf{I}_{BC_{down}}$ and $\mathbf{I}_{FC_{down}}$.

LC Decoding. In the decoder part, we combined the luminance and chrominance features from the encoder by adding them as a skip connection to guide the decoder’s LCGAB. The LCGAB in the decoder is followed by a transpose convolution operation to decode the RGB images into their actual input dimension.

$$\mathbf{I}_{L_{dec}} = LCGAB(\mathbf{I}_{BL_{down}}, \mathbf{I}_{FL_{down}}) \quad (9)$$

$$\mathbf{I}_{UP} = ConvTransposed(\mathbf{I}_{L_{dec}}) \quad (10)$$

Chrominance features are also up-sampled similarly. We refined the final decoded features with our reconstructed luminance and chrominance attributes. Additionally, our TFFormer is designed as a fully convolutional network and can take images of any dimension as input. It can generate the output with the same dimension as the input without losing any spatial dimension.

C.2. Loss calculation

To perceive visually pluisable images, we leverage an additional L1 loss along with the proposed LCPL. Thereby, we defined final LC-guided loss as:

$$\mathcal{L} = \lambda_R(\mathcal{L}_R + \mathcal{L}_{LC}) \quad (11)$$

where \mathcal{L}_R represents the traditional L_1 loss, λ_R is a low-light regularization coefficient.

C.3. Training Details

We implemented our proposed TFFormer using PyTorch framework [32]. Our TFFormer optimized with an Adam optimizer [18] with a hyperparameter of $\beta_1 = 0.9$, $\beta_2 = 0.99$. We set the initial learning rate = $1e - 4$ and adjusted it after training 100,000 steps using ReduceLRonPlateau scheduler [5]. We trained our model for 250,000 steps, utilizing a batch size of 12 and image dimensions $128 \times 128 \times 3$. Additionally, we leverage a low-light regularization coefficient $\lambda_R = 0.2$ empharically to tune the proposed LC guidance. The training process spanned approximately 100 hours, executed on low-end hardware featuring an AMD Ryzen 3200G central processing unit (CPU) operating at 3.6 GHz, complemented by 32 GB of random-access memory, and an Nvidia GeForce GTX 3060 (12GB) graphical processing unit (GPU).

C.4. TFFormer on SLLIE Datasets

To assess the performance of the proposed LSD dataset against existing SLLIE datasets, we leverage our TFFormer model throughout this study. Prior to conducting cross-dataset comparisons, we validated the effectiveness of TFFormer on existing SLLIE datasets to ensure a fair and consistent evaluation. For this purpose, we compared TFFormer with state-of-the-art (SOTA) SLLIE methods that utilize Retinex theory or transformer-based architectures. Tab. 11 summarizes these comparisons, focusing on methods like Retinexformer, recognized as one of the best single-stage SLLIE models and the winner of the NCLLIE-CVPR24 challenge. Additionally, we included only models for which reported results were reproducible.

As shown in Tab. 11, TFFormer consistently outperformed all SOTA methods across LOL-V1 [49] and LOL-V2 (real) [55] datasets. Specifically, TFFormer achieved the

highest PSNR (26.13 dB on LOL-V1 and 31.55 dB on LOL-V2), SSIM (0.8875 on LOL-V1 and 0.9147 on LOL-V2), and the lowest LPIPS (6.12 and 3.79, respectively). These results highlight the superior performance of TFFormer in enhancing real-world low-light images, surpassing strong baselines such as Retinexformer and MIRNet. This establishes TFFormer as a robust model for LSD-based evaluations and a strong contender for advancing SLLIE research on diverse datasets.

In addition to the quantitative evaluation, the qualitative results in Fig. 17 and Fig. 18 further demonstrate the practicability of TFFormer for generic SLLIE tasks. The proposed TFFormer consistently produces cleaner images with enhanced detail preservation and improved color accuracy, resembling the reference images. Additionally, the superior performance of TFFormer on LOL-V1 and LOL-V2 ensures its reliability and robustness for performing cross-dataset evaluations.

C.5. Inference Analysis

Tab. 12 demonstrates the inference speed and computational complexity of the proposed TFFormer on our hardware setup. Notably, the proposed TFFormer comprises only 5.87M trainable parameters—substantially fewer than those in well-known transformer models such as Uformer, MIRNet, and SNRNet. Moreover, as a single-stage network, TFFormer enables end-to-end optimization and efficient inference, enhancing performance while significantly reducing computational overhead. It takes just over 0.5 sec to enhance a large dimension low-light input on a mid-end GPU like GTX-3060. It is worth noting we evaluated our method with Float32 precision without performing any optimization. Therefore, the inference speed of TFFormer can be further improved by adopting model compression techniques such as quantization [54], pruning [21], etc., for future usage.

D. LSD-TFFormer In Real-world

This section illustrates more results of LSD-TFFormer on diverse scenarios.

D.1. TFFormer on LSD

Our TFFormer can perform evenly in numerous lighting conditions and scene types. We perform an extensive evaluation of TFFormer in eight subsets of LSD testing set. Fig. 19 and 20 illustrate the performance of our TFFormer in all subcategories of the proposed LSD pair benchmark dataset. Please note that the LSD benchmark dataset was collected using various camera sensors of different sizes. These sensors exhibit distinct responses to different lighting conditions. As a result, certain scenes within the LSD testing benchmark dataset may appear either darker or brighter than their actual lighting conditions.

D.2. LSD on Deep SLLIE Methods

The primary motivation of this study is to advance SLLIE methods by providing a reliable dataset for training deep-learning models on real-world scenarios and benchmarking their performance across diverse conditions. To evaluate this, we trained the state-of-the-art Retinexformer [4] on existing LOL-V1, LOL-V2, and our proposed LSD dataset. Subsequently, we tested the model on complex scenes out of this dataset. Fig. 21 illustrates the performance of Retinexformer in enhancing these real-world complex scenes.

Notably, Retinexformer is one of the top-performing methods on LOL-V1 and LOL-V2. However, we observed that even its pretrained model (obtained directly from the official repository) often produces severe artifacts and over-exposed regions in challenging scenarios trained with existing SLLIE datasets. In contrast, training Retinexformer on the proposed LSD dataset enables it to generate more natural and visually appealing results. Furthermore, our TFFormer surpasses its counterparts by producing cleaner and more plausible images, thanks to its LC Encoding and LC Guidance mechanisms. These results underline the significant contributions of the LSD dataset and TFFormer in tackling real-world SLLIE challenges and their practicability in improving SLLIE methods.

D.3. LSD-TFFormer on Real-world Scenes

Visual Comparison. Fig. 22 illustrates more examples of real-world SLLIE obtained by the proposed LSD-TFFormer. Our method can handle diverse scenes obtained by numerous hardware and lighting conditions. Our LSD-TFFormer is also effective in enhancing images stored on social media (e.g., Facebook, Twitter, Instagram, etc.). These popular social platforms contain billions of user images captured with old camera hardware in low-light conditions. Our proposed method opens a new life to these images by enhancing and providing them with a modern touch.

User Study. We also performed a separate user study to verify the mass acceptance of our LSD-TFFormer in real-world scenarios. In a user study, 35 evaluators aged 15 to 62 reviewed three random pairs per category (low-light vs. enhanced) based solely on aesthetic appeal, unaware of the study’s purpose. As shown in Tab. 13, over 82% of participants preferred images enhanced by LSD-TFFormer, with a particularly high preference for social media and older images, highlighting the model’s practical applicability to real-world SLLIE.

D.4. Visual Improvement on Vision Task

Apart from aesthetical use cases, the proposed method can also accelerate everyday vision tasks. Fig. 23 illustrates the performance gain achieved in two prominent vision tasks by incorporating our proposed method. Our approach sig-

Method	LOL-V1			LOL-V2			Average		
	PSNR \uparrow	SSIM \uparrow	LPIPS \downarrow	PSNR \uparrow	SSIM \uparrow	LPIPS \downarrow	PSNR \uparrow	SSIM \uparrow	LPIPS \downarrow
Input	7.77	0.4186	37.08	9.72	0.4370	27.24	8.75	0.4278	32.16
Kind [61]	19.66	0.8519	10.42	18.06	0.8571	12.59	18.86	0.8545	11.51
MIRNet [57]	24.14	0.8675	7.45	28.10	0.9012	5.13	26.12	0.8844	6.29
SNRNet [52]	24.61	0.8660	6.84	21.48	0.8717	9.15	23.05	0.8689	7.99
Retinexformer [4]	25.15	0.8675	6.54	22.79	0.8637	8.20	23.97	0.8656	7.37
TFFormer	26.13	0.8875	6.12	31.55	0.9147	3.79	28.84	0.9011	4.95

Table 11. Quantitive comparison between existing SLLIE methods and TFFormer on LOL-V1 and LOL-V2. The proposed TFFormer outperforms the existing methods on existing benchmarking datasets as well. The best and the second-best results are highlighted in red and blue, respectively.

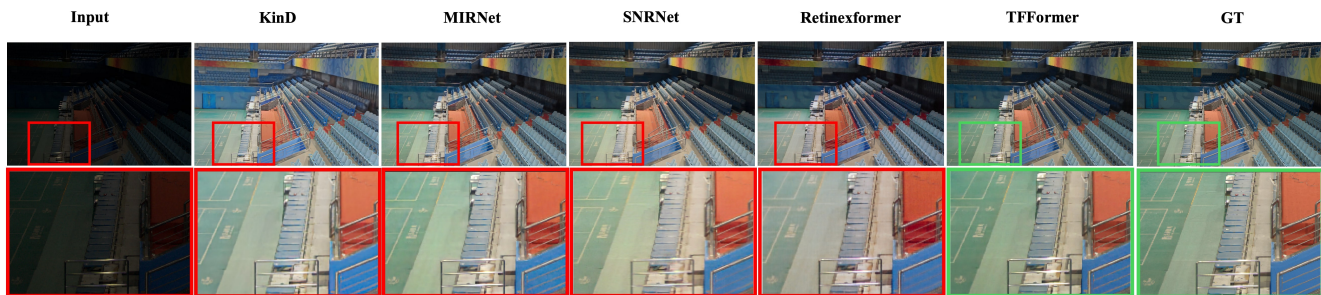


Figure 17. Qualitative comparison between TFFormer and SOTA methods. The proposed method can produce cleaner and more color-accurate indoor scene images.

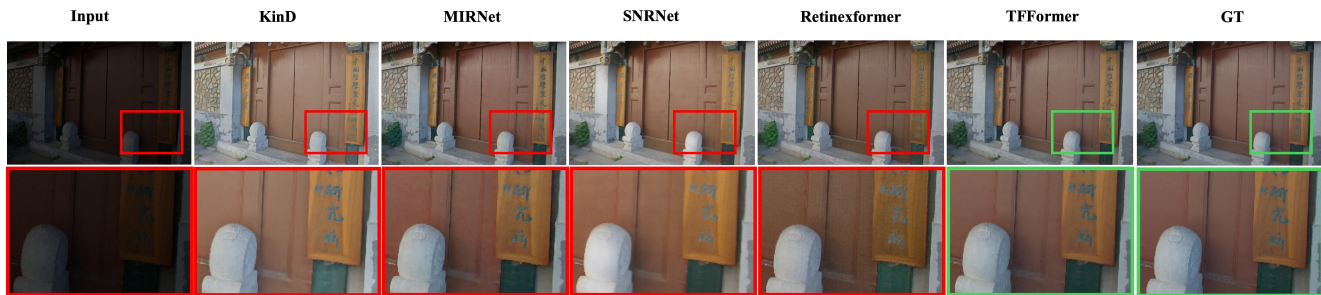


Figure 18. Qualitative comparison between TFFormer and SOTA methods. The proposed method can produce cleaner and more color-accurate images on outdoor scenes.

Input Size	Param. (M)	Compl. (GMac)	Inf. Time (ms)
$256 \times 256 \times 3$		34.52	62.21
$512 \times 512 \times 3$	5.87	138.09	180.37
$1024 \times 1024 \times 3$		552.35	657.78

Table 12. Inference analysis of proposed TFFormer.

nificantly enhances the performance of widely utilized object detection (OD) [44] algorithms and facilitates improved matching of images [34] in low-light conditions. Notably, matching and registering low-light and well-lit images to make a paired dataset for SLLIE is extremely difficult.

Device	Low-light \uparrow	LSD-TFFormer \uparrow
DSLR	0.0952	0.9048
Video (Frames)	0.3095	0.6905
iPhone	0.1905	0.8095
Android	0.2063	0.7937
Social Media	0.0714	0.9286
Average	0.1746	0.8254

Table 13. User study on LSD-TFFormer. In 82% of cases, user preferred LSD-TFFormer over low-light images.

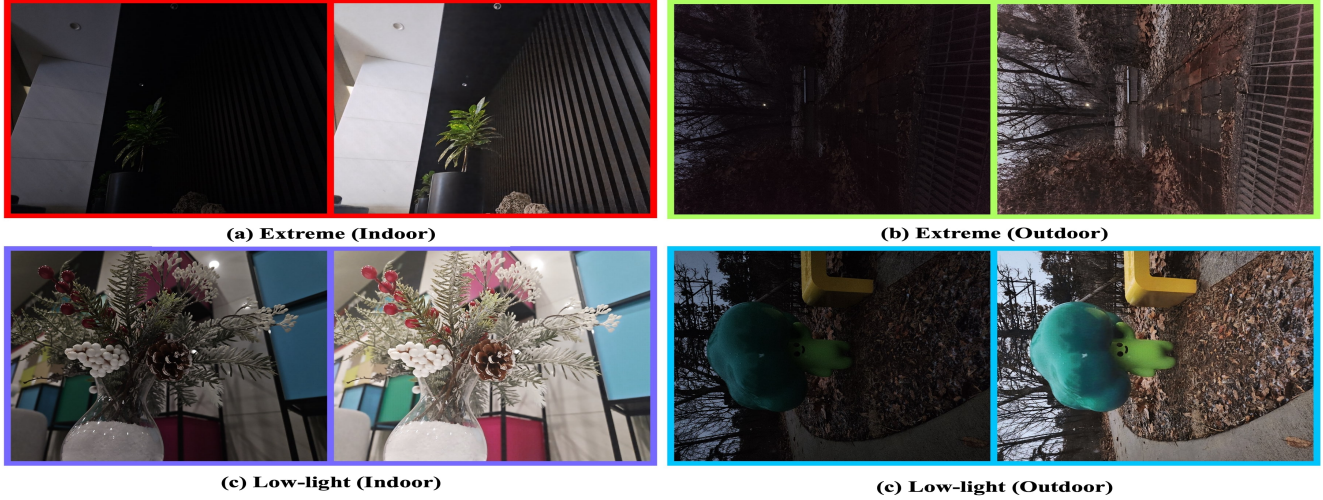


Figure 19. TFFormer performance on DLI subsets, including indoor and outdoor scenes from low-light and extreme lighting conditions. In each pair, on the left is the input image, and on the right is the enhanced image by LSD-TFFormer.

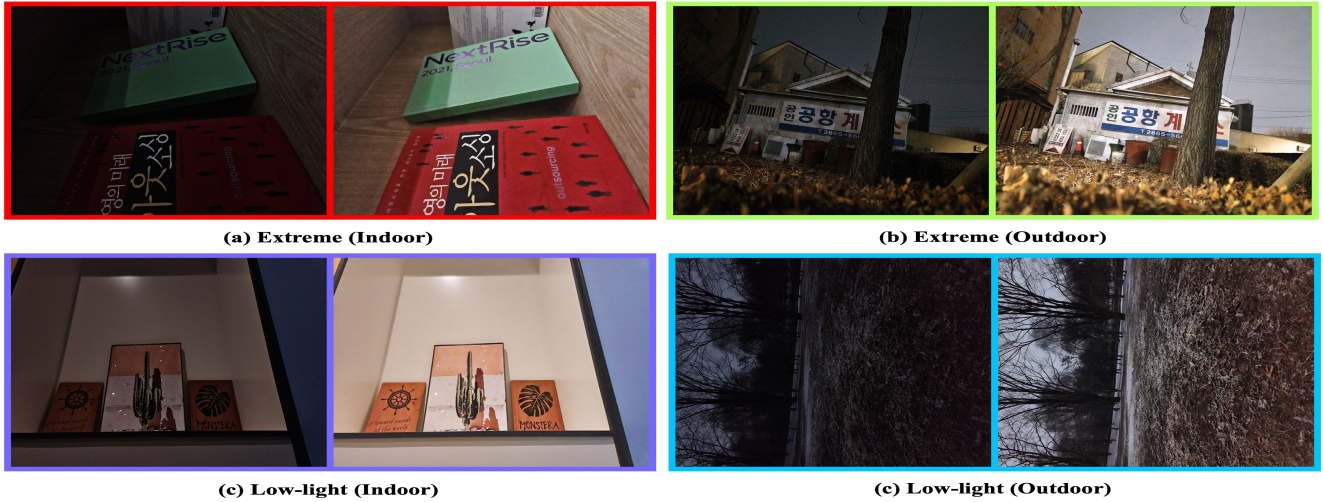


Figure 20. TFFormer performance on NLI subsets, including indoor and outdoor scenes from low-light and extreme lighting conditions. In each pair, on the left is the input image, and on the right is the enhanced image by LSD-TFFormer.

However, our method can support future studies by seamlessly matching collected low-light and well-lit images to enrich SLLIE research.

D.5. LSD-TFFormer vs Night mode

Night-mode photos are typically produced by combining multiple shots with different exposure settings. Comparing multi-shot approaches like night mode with single-shot methods such as LSD-TFFormer is unfair. However, to push the limit and study the feasibility of single-shot SLLIE in a broader aspect, we evaluated and compared our LSD-TFFormer with night mode photos. Thus, we mount our smartphone on a fixed point and fixed its focal point. Later,

we captured one scene in auto mode and another by enabling the dedicated night mode.

We enhanced the auto-mode photo (without night mode) with our LSD-TFFormer. Fig. 24 illustrates the comparison between LSD-TFFormer and night mode from Samsung Galaxy Z fold 5. We found that such dedicated night photography mode of smartphones is a trend to produce smooth images that lack salient details. On the other hand, our method can produce brighter images compared to the multi-shot processing while maintaining the salient details of the short-exposure images.

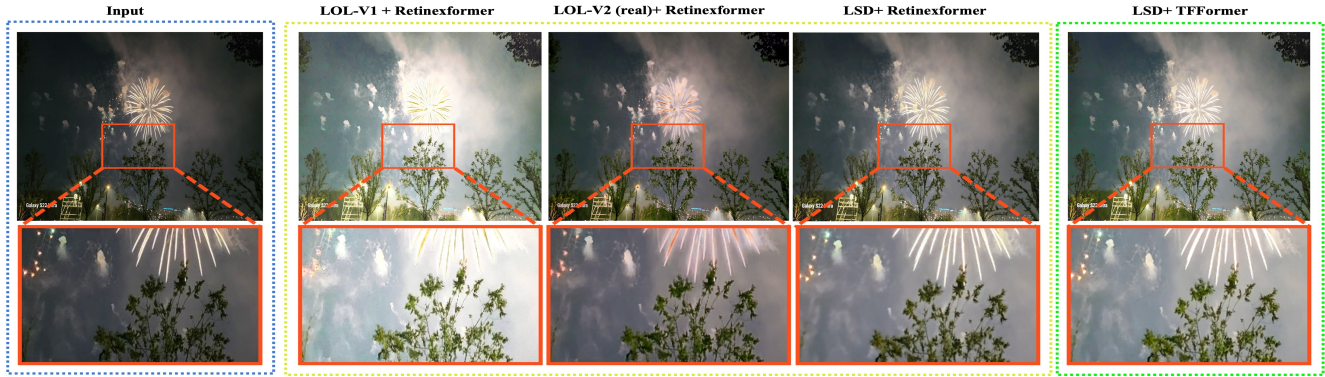


Figure 21. Real-world complex scene enhancement with low-light image enhancement methods. (a) input image capture with Samsung S22 Ultra. (b)-(c) Retinexformer[4] with existing datasets. (d) Retinexformer[4] with LSD. (e) Proposed (LSD-TFFormer)

D.6. Failure Case

Despite promising results in numerous test cases, our TFFormer can produce visible noisy regions in NLL scenes captured under 1 lux. Fig. 25 illustrates such an example of a failure case. We planned to address such extremely challenging cases in future studies.

References

- [1] Ralph Allan Bradley and Milton E Terry. Rank analysis of incomplete block designs: I. the method of paired comparisons. *Biometrika*, 39(3/4):324–345, 1952. 6
- [2] Jianrui Cai, Shuhang Gu, and Lei Zhang. Learning a deep single image contrast enhancer from multi-exposure images. *IEEE Transactions on Image Processing*, 27(4):2049–2062, 2018. 1
- [3] Yuanhao Cai, Jing Lin, Haoqian Wang, Xin Yuan, Henghui Ding, Yulun Zhang, Radu Timofte, and Luc V Gool. Degradation-aware unfolding half-shuffle transformer for spectral compressive imaging. *Advances in Neural Information Processing Systems*, 35:37749–37761, 2022. 2
- [4] Yuanhao Cai, Hao Bian, Jing Lin, Haoqian Wang, Radu Timofte, and Yulun Zhang. Retinexformer: One-stage retinex-based transformer for low-light image enhancement. *arXiv preprint arXiv:2303.06705*, 2023. 1, 4, 5, 6, 14, 15, 17
- [5] PyTorch Contributors. Pytorch documentation - torch.optim.lr_scheduler.reduceLrOnPlateau, 2024. Accessed on 2024-03-02. 13
- [6] PyTorch Contributors. Models and pre-trained weights, 2024. Accessed on 2024-03-10. 9
- [7] Z Cui, K Li, L Gu, S Su, P Gao, Z Jiang, Y Qiao, and T Harada. You only need 90k parameters to adapt light: A light weight transformer for image enhancement and exposure correction. arxiv 2022. *arXiv preprint arXiv:2205.14871*, 238, 2022. 1, 6
- [8] Jia Deng, Wei Dong, Richard Socher, Li-Jia Li, Kai Li, and Li Fei-Fei. Imagenet: A large-scale hierarchical image database. In *2009 IEEE conference on computer vision and pattern recognition*, pages 248–255. Ieee, 2009. 9
- [9] Saijie Fan, Wei Liang, Derui Ding, and Hui Yu. Lacn: A lightweight attention-guided convnext network for low-light image enhancement. *Engineering Applications of Artificial Intelligence*, 117:105632, 2023. 1
- [10] Ali Farhadi and Joseph Redmon. Yolov3: An incremental improvement. In *Computer vision and pattern recognition*, pages 1–6. Springer Berlin/Heidelberg, Germany, 2018. 7
- [11] Zhenqi Fu, Yan Yang, Xiaotong Tu, Yue Huang, Xinghao Ding, and Kai-Kuang Ma. Learning a simple low-light image enhancer from paired low-light instances. In *Proceedings of the IEEE/CVF Conference on Computer Vision and Pattern Recognition*, pages 22252–22261, 2023. 1
- [12] Google. Android camera api documentation, 2024. Accessed on 2024-03-02. 3, 9
- [13] Jiang Hai, Zhu Xuan, Ren Yang, Yutong Hao, Fengzhu Zou, Fang Lin, and Songchen Han. R2rnet: Low-light image enhancement via real-low to real-normal network. *Journal of Visual Communication and Image Representation*, 90: 103712, 2023. 1, 2, 3, 7
- [14] Gao Huang, Zhuang Liu, Laurens Van Der Maaten, and Kilian Q Weinberger. Densely connected convolutional networks. In *Proceedings of the IEEE conference on computer vision and pattern recognition*, pages 4700–4708, 2017. 10
- [15] Xin Jin, Ling-Hao Han, Zhen Li, Chun-Le Guo, Zhi Chai, and Chongyi Li. Dnf: Decouple and feedback network for seeing in the dark. In *Proceedings of the IEEE/CVF Conference on Computer Vision and Pattern Recognition*, pages 18135–18144, 2023. 1
- [16] Min H Kim, Tim Weyrich, and Jan Kautz. Modeling human color perception under extended luminance levels. In *ACM SIGGRAPH 2009 papers*, pages 1–9. 2009. 2
- [17] Wonjun Kim. Low-light image enhancement: A comparative review and prospects. *IEEE Access*, 2022. 1
- [18] Diederik P Kingma and Jimmy Ba. Adam: A method for stochastic optimization. *arXiv preprint arXiv:1412.6980*, 2014. 13
- [19] Edwin H Land and John J McCann. Lightness and retinex theory. *Josa*, 61(1):1–11, 1971. 1
- [20] Chongyi Li, Chunle Guo, Linghao Han, Jun Jiang, Ming-Ming Cheng, Jinwei Gu, and Chen Change Loy. Low-light

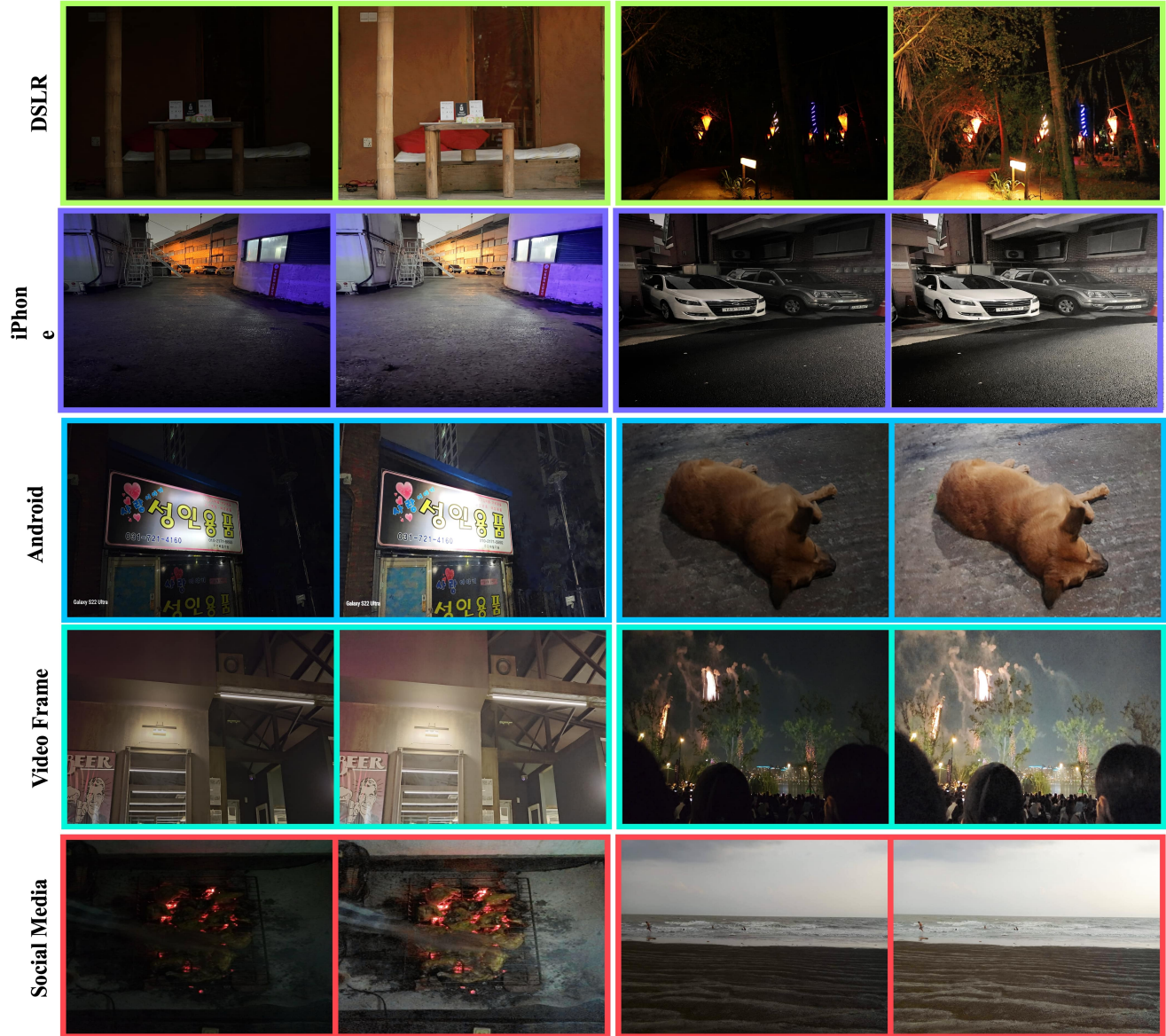


Figure 22. Few more examples of generic SLLIE obtained by LSD-TFFormer. In each pair, on the left is the input image, and on the right is the enhanced image by LSD-TFFormer.

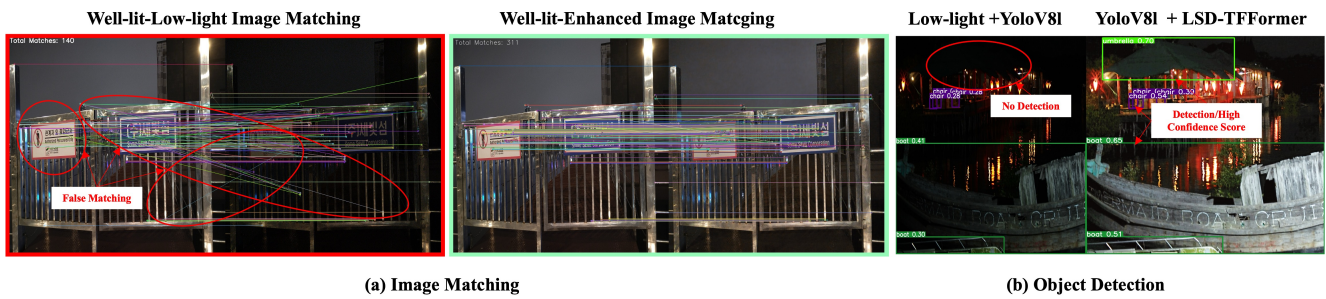


Figure 23. LSD-TFFormer usability in vision tasks. (a) Image matching. (b) Object Detection

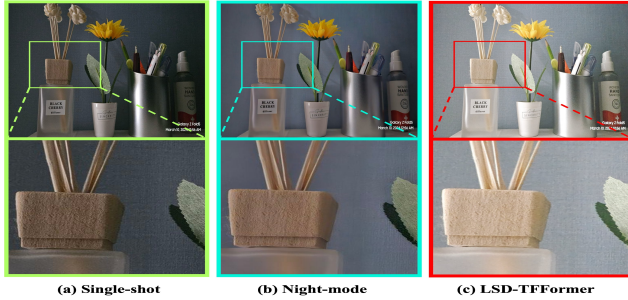


Figure 24. Comparison between LSD-TFFormer and night mode. Scenes capture under 20 lux with Samsung Galaxy Z fold 5. (a) Z Fold 5 without night mode. (b) Z Fold 5 with night mode. (c) Z Fold 5 without night mode scene enhanced by LSD-TFFormer.



Figure 25. Example of failure case. For NLL scenes, TFFormer can illustrate visible noise in some extreme cases (e.g., under 1 lux). Left: NLL input (under 1 lux), right: LSD-TFFormer.

image and video enhancement using deep learning: A survey. *IEEE transactions on pattern analysis and machine intelligence*, 44(12):9396–9416, 2021. 3

[21] Lianqiang Li, Jie Zhu, and Ming-Ting Sun. Deep learning based method for pruning deep neural networks. In *2019 IEEE International Conference on Multimedia & Expo Workshops (ICMEW)*, pages 312–317. IEEE, 2019. 14

[22] Yuhang Li, Tianyanshi Liu, Jiabin Fan, and Youdong Ding. Ldnet: low-light image enhancement with joint lighting and denoising. *Machine Vision and Applications*, 34(1):13, 2023. 1

[23] Chiunhsiun Lin. Face detection in complicated backgrounds and different illumination conditions by using ycbcr color space and neural network. *Pattern Recognition Letters*, 28(16):2190–2200, 2007. 4

[24] Jiaying Liu, Dejie Xu, Wenhan Yang, Minhao Fan, and Haofeng Huang. Benchmarking low-light image enhancement and beyond. *International Journal of Computer Vision*, 129:1153–1184, 2021. 3

[25] Shuying Liu and Weihong Deng. Very deep convolutional neural network based image classification using small training sample size. In *2015 3rd IAPR Asian conference on pattern recognition (ACPR)*, pages 730–734. IEEE, 2015. 4, 10

[26] Xiaokai Liu, Weihao Ma, Xiaorui Ma, and Jie Wang. Lae-net: a locally-adaptive embedding network for low-light im-

age enhancement. *Pattern Recognition*, 133:109039, 2023. 1

[27] Xiaoning Liu, Zongwei Wu, Ao Li, Florin-Alexandru Vasluianu, Yulun Zhang, Shuhang Gu, Le Zhang, Ce Zhu, Radu Timofte, Zhi Jin, et al. Ntire 2024 challenge on low light image enhancement: Methods and results. *arXiv preprint arXiv:2404.14248*, 2024. 1, 2, 3, 7

[28] Yuen Peng Loh and Chee Seng Chan. Getting to know low-light images with the exclusively dark dataset. *Computer Vision and Image Understanding*, 178:30–42, 2019. 7

[29] Kin Gwn Lore, Adedotun Akintayo, and Soumik Sarkar. Llnet: A deep autoencoder approach to natural low-light image enhancement. *Pattern Recognition*, 61:650–662, 2017. 1

[30] Yucheng Lu, Dong-Wook Kim, and Seung-Won Jung. Deepselfie: Single-shot low-light enhancement for selfies. *IEEE Access*, 8:121424–121436, 2020. 1

[31] Carlos Alejandro Párraga, Gavin Brelstaff, Tom Troscianko, and IR Moorehead. Color and luminance information in natural scenes. *Journal of the Optical Society of America A*, 15(3):563–569, 1998. 2

[32] Pytorch. PyTorch Framework code. <https://pytorch.org/>, 2016. Accessed: 2020-08-24. 13

[33] Junxiang Ruan, Xiangtao Kong, Wenqi Huang, and Wenming Yang. Retiformer: retinex-based enhancement in transformer for low-light image. In *ICASSP 2023-2023 IEEE International Conference on Acoustics, Speech and Signal Processing (ICASSP)*, pages 1–5. IEEE, 2023. 1

[34] Ethan Rublee, Vincent Rabaud, Kurt Konolige, and Gary R. Bradski. Orb: An efficient alternative to sift or surf. In *2011 International Conference on Computer Vision (ICCV)*, pages 2564–2571, 2011. 15

[35] Yunxue Shao, Yijin Diao, and Lingfeng Wang. Rpa: A performer-based retinex model for low-light image enhancement. 2025. 1

[36] Dori Shapira, Shai Avidan, and Yacov Hel-Or. Multiple histogram matching. In *2013 IEEE international conference on image processing*, pages 2269–2273. IEEE, 2013. 3

[37] SMA Sharif, Rizwan Ali Naqvi, Farman Ali, and Mithun Biswas. Darkdeblur: Learning single-shot image deblurring in low-light condition. *Expert Systems with Applications*, 222:119739, 2023. 1

[38] Dinggang Shen. Image registration by local histogram matching. *Pattern Recognition*, 40(4):1161–1172, 2007. 3

[39] Liang Shen, Zihan Yue, Fan Feng, Quan Chen, Shihao Liu, and Jie Ma. Msr-net: Low-light image enhancement using deep convolutional network. *arXiv preprint arXiv:1711.02488*, 2017. 1

[40] Kavinder Singh and Anil Singh Parihar. Illumination estimation for nature preserving low-light image enhancement. *The Visual Computer*, 40(1):121–136, 2024. 1

[41] Sushant Singh and Ausif Mahmood. The nlp cookbook: modern recipes for transformer based deep learning architectures. *IEEE Access*, 9:68675–68702, 2021. 1, 2

[42] Vishnu Subramanian. *Deep Learning with PyTorch: A practical approach to building neural network models using PyTorch*. Packt Publishing Ltd, 2018. 9

- [43] Li Tao, Chuang Zhu, Guoqing Xiang, Yuan Li, Huizhu Jia, and Xiaodong Xie. Llcn: A convolutional neural network for low-light image enhancement. In *2017 IEEE Visual Communications and Image Processing (VCIP)*, pages 1–4. IEEE, 2017. 1
- [44] Ultralytics. Ultralytics github repository. <https://github.com/ultralytics/ultralytics>, 2024. Accessed on 2024-03-02. 15
- [45] A Vaswani. Attention is all you need. *Advances in Neural Information Processing Systems*, 2017. 5
- [46] Ruixing Wang, Qing Zhang, Chi-Wing Fu, Xiaoyong Shen, Wei-Shi Zheng, and Jiaya Jia. Underexposed photo enhancement using deep illumination estimation. In *The IEEE Conference on Computer Vision and Pattern Recognition (CVPR)*, 2019. 1
- [47] Ruixing Wang, Qing Zhang, Chi-Wing Fu, Xiaoyong Shen, Wei-Shi Zheng, and Jiaya Jia. Underexposed photo enhancement using deep illumination estimation. In *Proceedings of the IEEE/CVF conference on computer vision and pattern recognition*, pages 6849–6857, 2019. 1, 6
- [48] Zhendong Wang, Xiaodong Cun, Jianmin Bao, Wengang Zhou, Jianzhuang Liu, and Houqiang Li. Uformer: A general u-shaped transformer for image restoration. In *Proceedings of the IEEE/CVF conference on computer vision and pattern recognition*, pages 17683–17693, 2022. 1, 2, 5, 6
- [49] Chen Wei, Wenjing Wang, Wenhan Yang, and Jiaying Liu. Deep retinex decomposition for low-light enhancement. *arXiv preprint arXiv:1808.04560*, 2018. 1, 2, 3, 6, 7, 13
- [50] Wenhui Wu, Jian Weng, Pingping Zhang, Xu Wang, Wenhan Yang, and Jianmin Jiang. Uretinex-net: Retinex-based deep unfolding network for low-light image enhancement. In *Proceedings of the IEEE/CVF conference on computer vision and pattern recognition*, pages 5901–5910, 2022. 1
- [51] Zifeng Wu, Chunhua Shen, and Anton Van Den Hengel. Wider or deeper: Revisiting the resnet model for visual recognition. *Pattern recognition*, 90:119–133, 2019. 10
- [52] Xiaogang Xu, Ruixing Wang, Chi-Wing Fu, and Jiaya Jia. Snr-aware low-light image enhancement. In *Proceedings of the IEEE/CVF conference on computer vision and pattern recognition*, pages 17714–17724, 2022. 1, 5, 6, 15
- [53] Xiaogang Xu, Ruixing Wang, and Jiangbo Lu. Low-light image enhancement via structure modeling and guidance. In *Proceedings of the IEEE/CVF Conference on Computer Vision and Pattern Recognition*, pages 9893–9903, 2023. 1
- [54] Jiwei Yang, Xu Shen, Jun Xing, Xinmei Tian, Houqiang Li, Bing Deng, Jianqiang Huang, and Xian-sheng Hua. Quantization networks. In *Proceedings of the IEEE/CVF conference on computer vision and pattern recognition*, pages 7308–7316, 2019. 14
- [55] Wenhan Yang, Wenjing Wang, Haofeng Huang, Shiqi Wang, and Jiaying Liu. Sparse gradient regularized deep retinex network for robust low-light image enhancement. *IEEE Transactions on Image Processing*, 30:2072–2086, 2021. 1, 2, 3, 7, 13
- [56] Xunpeng Yi, Han Xu, Hao Zhang, Linfeng Tang, and Jiayi Ma. Diff-retinex: Rethinking low-light image enhancement with a generative diffusion model. In *Proceedings of the IEEE/CVF International Conference on Computer Vision*, pages 12302–12311, 2023. 1
- [57] Syed Waqas Zamir, Aditya Arora, Salman Khan, Munawar Hayat, Fahad Shahbaz Khan, Ming-Hsuan Yang, and Ling Shao. Learning enriched features for real image restoration and enhancement. In *Computer Vision—ECCV 2020: 16th European Conference, Glasgow, UK, August 23–28, 2020, Proceedings, Part XXV 16*, pages 492–511. Springer, 2020. 1, 6, 15
- [58] Syed Waqas Zamir, Aditya Arora, Salman Khan, Munawar Hayat, Fahad Shahbaz Khan, and Ming-Hsuan Yang. Restormer: Efficient transformer for high-resolution image restoration. In *Proceedings of the IEEE/CVF conference on computer vision and pattern recognition*, pages 5728–5739, 2022. 1
- [59] Fan Zhang, Yu Li, Shaodi You, and Ying Fu. Learning temporal consistency for low light video enhancement from single images. In *Proceedings of the IEEE/CVF conference on computer vision and pattern recognition*, pages 4967–4976, 2021. 1
- [60] Qing Zhang, Yongwei Nie, and Wei-Shi Zheng. Dual illumination estimation for robust exposure correction. In *Computer graphics forum*, pages 243–252. Wiley Online Library, 2019. 1
- [61] Yonghua Zhang, Jiawan Zhang, and Xiaojie Guo. Kindling the darkness: A practical low-light image enhancer. In *Proceedings of the 27th ACM international conference on multimedia*, pages 1632–1640, 2019. 6, 15
- [62] Yonghua Zhang, Xiaojie Guo, Jiayi Ma, Wei Liu, and Jiawan Zhang. Beyond brightening low-light images. *International Journal of Computer Vision*, 129:1013–1037, 2021. 1, 6
- [63] Zunjin Zhao, Bangshu Xiong, Lei Wang, Qiaofeng Ou, Lei Yu, and Fa Kuang. Retinexdip: A unified deep framework for low-light image enhancement. *IEEE Transactions on Circuits and Systems for Video Technology*, 32(3):1076–1088, 2021. 1
- [64] Chu Zhou, Minggui Teng, Jin Han, Chao Xu, and Boxin Shi. Delieve-net: Deblurring low-light images with light streaks and local events. In *Proceedings of the IEEE/CVF International Conference on Computer Vision*, pages 1155–1164, 2021. 1
- [65] Xia Zhu, Renwen Chen, Huakang Xia, and Piaoyan Zhang. Shadow removal based on ycbcr color space. *Neurocomputing*, 151:252–258, 2015. 4